

1 **Supporting Information**

2 for

3 **A high-resolution Global Aviation emissions Inventory based on ADS-B**
4 **(GAIA) for 2019 – 2021**

5
6 Roger Teoh¹, Zebediah Engberg², Marc Shapiro², Lynnette Dray³ and Marc E.J. Stettler^{1*}

7 ¹ Centre for Transport Studies, Department of Civil and Environmental Engineering, Imperial College London,
8 London, SW7 2AZ, United Kingdom

9 ² Breakthrough Energy, 4110 Carillon Point, Kirkland, WA 98033, United States

10 ³ Air Transportation Systems Laboratory, School of Environment, Energy and Resources, University College
11 London, London, WC1E 6BT, United Kingdom

12
13
14 * Corresponding author: m.stettler@imperial.ac.uk

15
16
17 Supporting Information Details:

- 18 • Number of pages: 48
19 • Number of figures: 21
20 • Number of tables: 13

| | | |
|----|-----------------|--|
| 21 | Contents | |
| 22 | S1 | Air Traffic Dataset3 |
| 23 | S1.1 | Background information.....3 |
| 24 | S1.2 | Data cleaning and trajectory completion5 |
| 25 | S1.3 | Summary statistics & validation..... 11 |
| 26 | S2 | Aircraft-engine combination..... 16 |
| 27 | S3 | Passenger Load Factor21 |
| 28 | S4 | nvPM emissions25 |
| 29 | S4.1 | T_4/T_2 methodology25 |
| 30 | S4.2 | Fractal aggregates model28 |
| 31 | S5 | Global aviation emissions inventory29 |
| 32 | S6 | Comparison with other studies.....35 |
| 33 | | References.....44 |
| 34 | | |
| 35 | | |

36 **S1 Air Traffic Dataset**

37 **S1.1 Background information**

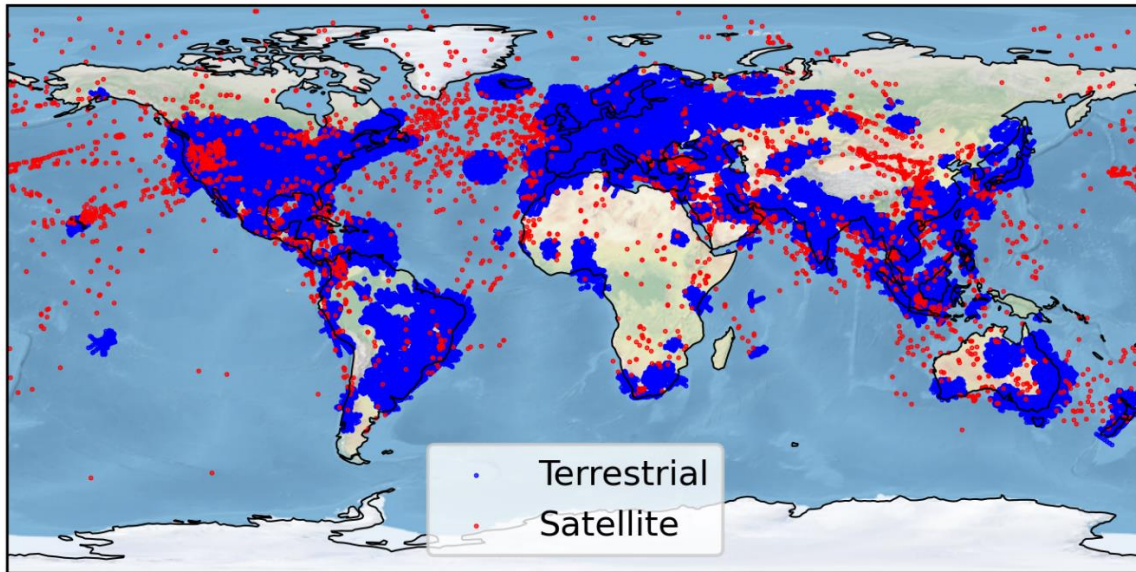
38 Aircraft that are equipped with an ADS-B transponder broadcast their precise location at a rate
39 of twice per second (ICAO, 2021a), and the following information is provided for each data
40 point:

- 41 • unique aircraft identifier, which includes the International Civil Aviation Organization
42 (ICAO) 24-bit aircraft address and call sign,
- 43 • GPS position (longitude and latitude),
- 44 • barometric altitude,
- 45 • aircraft heading,
- 46 • ground speed, and
- 47 • timestamp when the ADS-B signal is received.

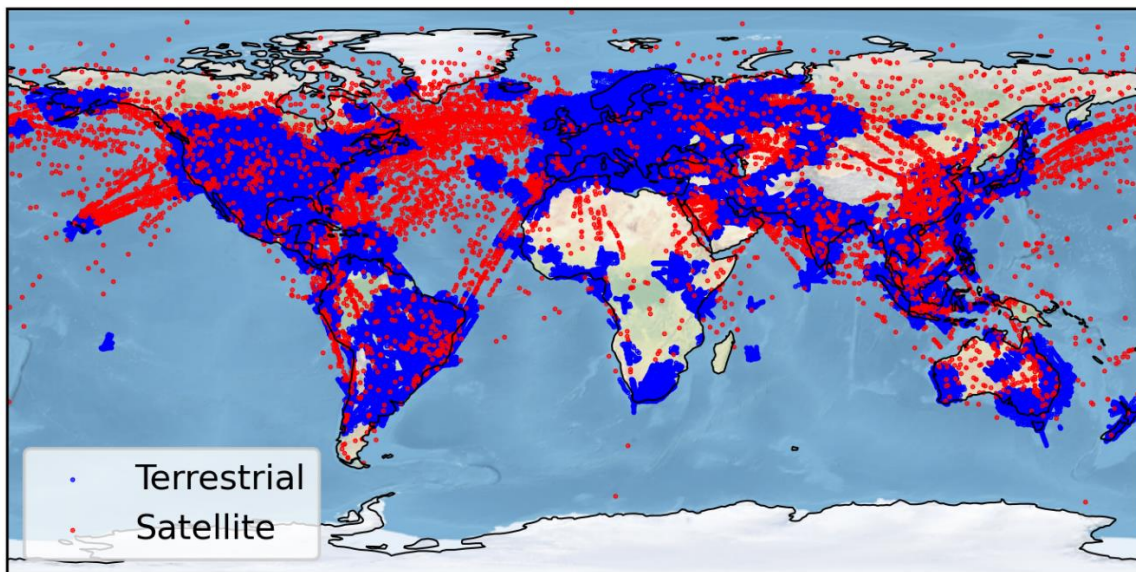
48 For the purposes of this research, we purchased an aircraft activity dataset from Spire Aviation
49 (n.d.) that contains global coverage of aircraft ADS-B telemetry data from 2019 to 2021 that
50 contains the variables listed above. Spire Aviation collects these ADS-B signals using a
51 combination of terrestrial receivers and its own satellite constellation, where ADS-B signals
52 from terrestrial receivers were provided at a temporal resolution of 300 s. The raw ADS-B data
53 is subsequently enriched by Spire Aviation with third-party aircraft database sources and flight
54 schedules to include additional flight-level information such as the:

- 55 • International Air Transport Association (IATA) flight number,
- 56 • aircraft tail number,
- 57 • ICAO aircraft type designator,
- 58 • ICAO airport code for the origin and destination airports, and
- 59 • scheduled and estimated departure and arrival time.

(a) 2019-01-01



(b) 2021-12-31



60

61 **Figure S1: Aircraft GPS positions that are provided by the ADS-B dataset on the (a) 1-January-2019; and**
62 **(b) 31-December-2021. Data points that are collected by terrestrial and satellite receivers are marked in**
63 **blue and red respectively. Basemap plotted using Cartopy 0.21.1 © Natural Earth; license: public domain.**

64 The aircraft activity dataset, hereby known as the ADS-B dataset, was selected ahead of other

65 ADS-B providers (such as Flightradar24, FlightAware and the OpenSky network) because of

66 the availability of satellite coverage and price affordability. Fig. S1 presents the aircraft GPS

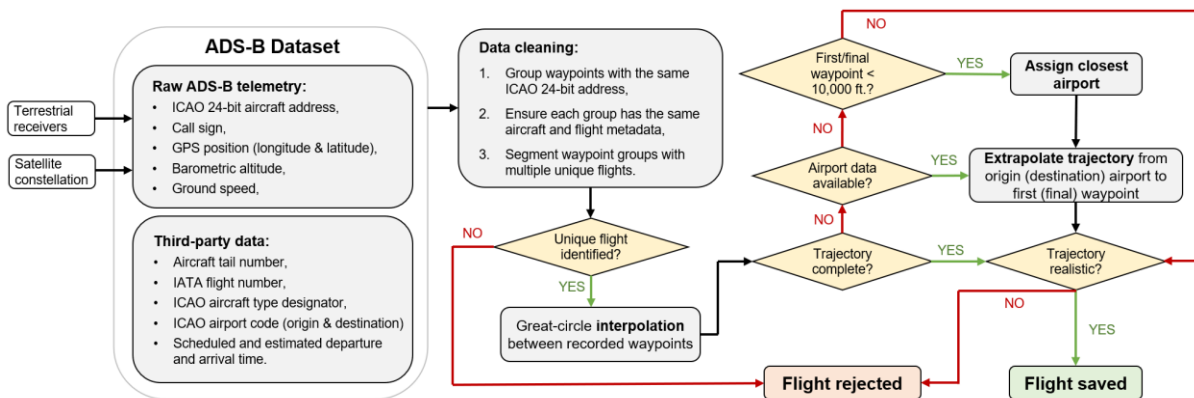
67 positions that are provided by the ADS-B dataset on 1-January-2019 and 31-December-2021,

68 showing that: (i) satellite-based ADS-B receivers enables flights to be tracked in regions that

69 previously had minimal radar coverage, for example, over the oceans, deserts, and mountain
 70 ranges; and (ii) an increasing coverage area of ADS-B receiver networks over time.

71 **S1.2 Data cleaning and trajectory completion**

72 The ICAO 24-bit aircraft address and call sign are used to identify unique flights in the ADS-
 73 B tracking data. It is not possible to identify the unique trajectories from individual flights using
 74 the raw ADS-B data because multiple unique flights can share the same identifier and/or can
 75 be airborne at the same time in rare instances. Here, we develop a workflow to: (i) identify the
 76 presence of multiple unique flights with the same ICAO address/call sign; (ii) group the
 77 waypoints that belong to distinctive flights to construct their trajectories for fuel consumption
 78 and emissions modelling; and (iii) fill any missing flight segments whenever possible. Fig. S2
 79 summarises the workflow that is developed to process the raw ADS-B dataset.



80
 81 **Figure S2: Data cleaning and trajectory completion workflow that is used to process the raw ADS-B**
 82 **dataset.**

83 The first step involves grouping waypoints by their ICAO 24-bit address. For each group, the
 84 number of unique flights (n) are identified when the set of waypoints have more than one
 85 unique call sign, aircraft type, origin-destination airport pair, and/or tail number. If $n > 1$, the
 86 waypoints are segmented to n sub-groups so that each subgroup have the same aircraft and
 87 flight properties. The subgroup of waypoints with missing, anonymised and/or unidentifiable
 88 aircraft types, such as rotorcraft and/or sensitive military flights, are beyond the scope of this

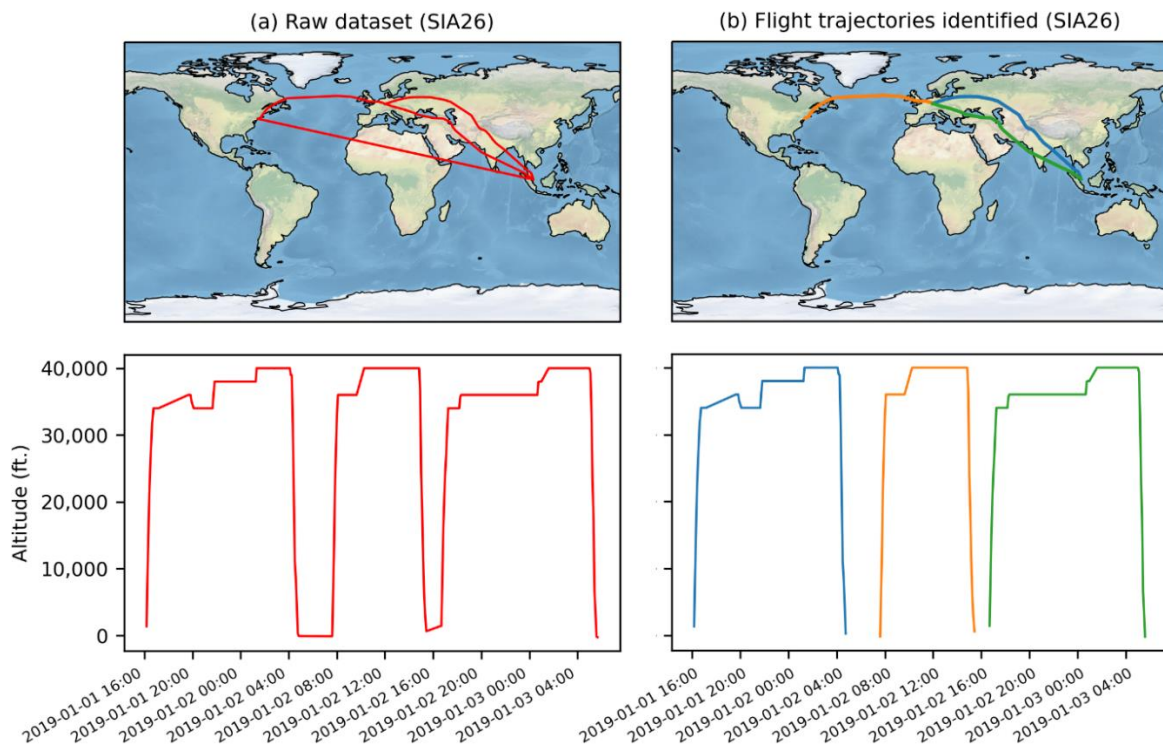
89 study and removed from the database. For each subgroup of waypoints, the algorithm performs
90 additional tests with the following rules to ensure that the constructed flight trajectories are
91 realistic:

- 92 1. the flight trajectory must consist of at least three recorded waypoints,
- 93 2. if airport metadata is available, the total flight segment length of the recorded waypoints
94 must be greater than 5% of the distance between the origin-destination airport pair,
- 95 3. the segment length between recorded waypoints must not be greater than the great-
96 circle distance between the origin-destination airport, or greater than 5000 km if the
97 airport data is not available,
- 98 4. the time difference between recorded waypoints (dt) must not be greater than the time
99 required to travel the great-circle distance between the origin-destination airport
100 (assuming a mean cruise speed of 180 m s^{-1} for jet aircraft and 70 m s^{-1} for turboprops
101 and piston aircraft), or greater than 6 h if the airport data is not available,
- 102 5. the estimated ground speed between waypoints must be within a reasonable range of
103 $100\text{--}350 \text{ m s}^{-1}$ when the flight is above 10,000 feet, or $20\text{--}300 \text{ m s}^{-1}$ when the flight is
104 below 10,000 feet,
- 105 6. check the altitude of waypoints during the cruise phase of flight, defined when the
106 altitude is above 50% of the service ceiling altitude of the aircraft type and the rate of
107 climb and descent (ROCD) is between ± 250 feet per minute. Unless there is a flight
108 diversion, waypoints between the beginning and end of the cruise phase of flight should
109 not be below 10,000 feet. For flights without a cruise phase of flight, the total flight
110 duration must not be greater than 2 h, which is used as an indication that it could be a
111 short-haul flight.

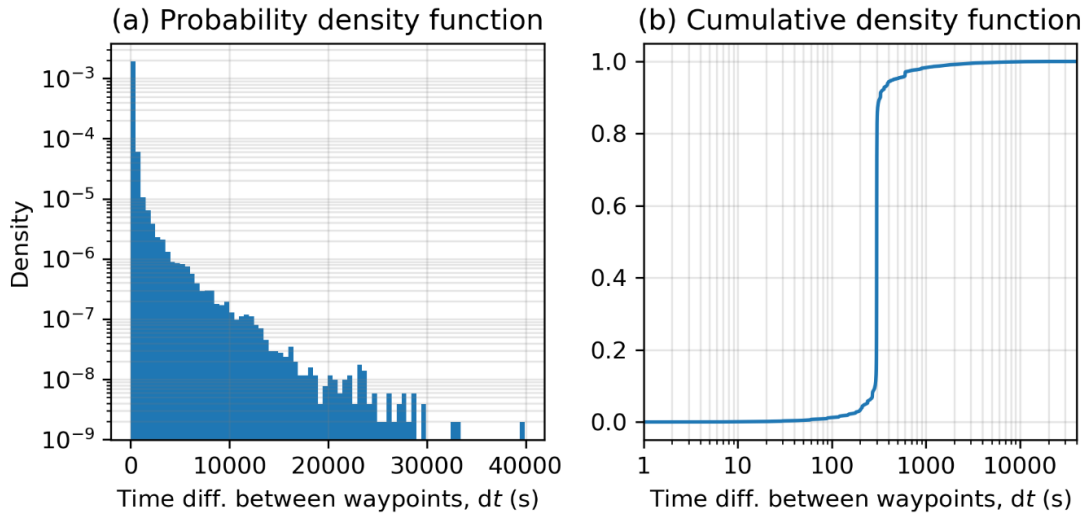
112 The subset of waypoints that violate conditions (1) and (2) are rejected as there is insufficient
113 data to construct a flight segment and trajectory. Multiple unique flights are identified when

114 conditions (3), (4), (5) and/or (6) are violated, and the waypoints are segmented at the flagged
115 waypoints. For condition (6), the presence of flight diversion is identified when all of the
116 following three conditions are satisfied:

- 117 • for flagged waypoints that should be at cruise (< 10,000 feet between the beginning and
118 end of the identified cruise phase of flight), their respective dt must be less than the
119 minimum aircraft turnaround time (i.e., duration between landing and take-off for a
120 new flight) that is set at 10 minutes,
- 121 • the segment length between the flagged waypoints must be greater than 1 km, which
122 indicates that the aircraft is airborne during this period, and
- 123 • the time elapsed between the flagged waypoints with the lowest altitude and the final
124 recorded waypoint should be less than 2 h.



125
126 **Figure S3: Example of (a) multiple unique flights sharing the same call sign in the unprocessed ADS-B**
127 **dataset; and the (b) segmented trajectories into three distinctive flights. The call sign, SIA26, is used for the**
128 **Singapore – Frankfurt – New York route that is operated by Singapore Airlines. Basemap plotted using**
129 **Cartopy 0.21.1 © Natural Earth; license: public domain.**

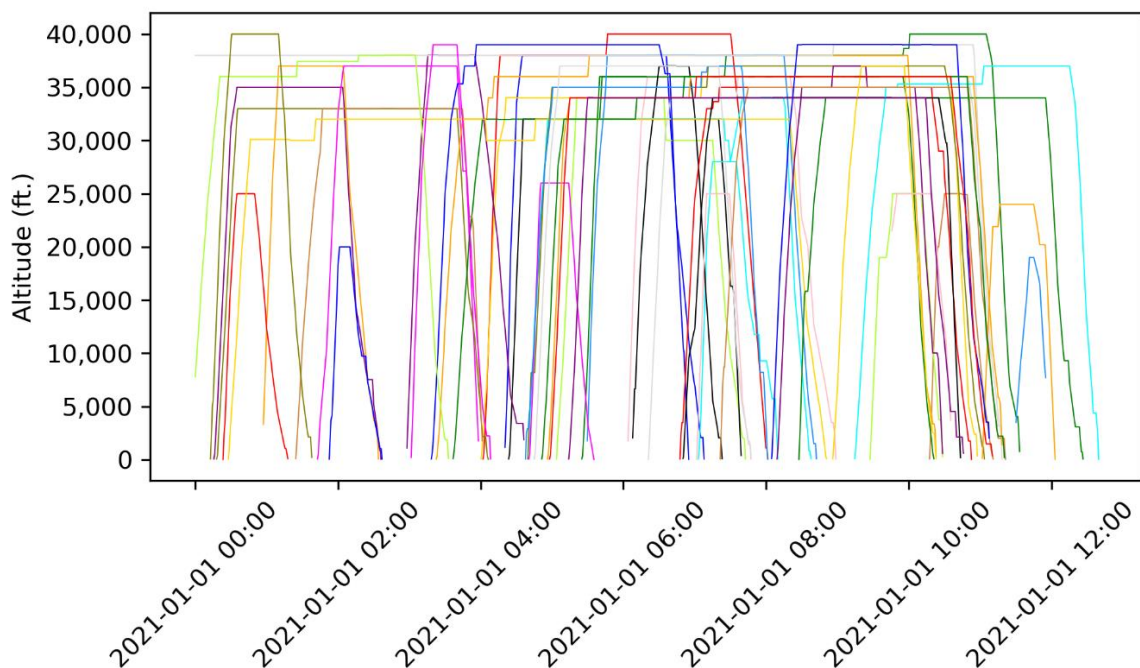


130

131 **Figure S4: The (a) probability density function and (b) cumulative density function on the time difference**
 132 **between recorded waypoints (dt) in the raw ADS-B dataset.**

133 Fig. S3 provides an example of multiple unique flights sharing the same call sign in the raw
 134 ADS-B dataset, and the data cleaning algorithm successfully identified and segmented the
 135 waypoints into three distinctive flights. Around 90% of the waypoints have a $dt < 300$ s when
 136 the aircraft is within the coverage of terrestrial receivers, but dt can be up to 40000 s (~ 11 h)
 137 when satellite data is not available (Fig. S4). For fuel consumption, emissions, and contrail
 138 modelling, a smaller dt is necessary to account for variations in ambient meteorology and
 139 aircraft performance over large length scales. On this basis, we perform a great-circle
 140 interpolation between the recorded waypoints to produce comparable segment lengths with dt
 141 ranging between 40 and 60 s. The great-circle interpolation also explicitly accounts for
 142 differences in altitude between the recorded waypoints. When the altitude between two
 143 successive waypoints is not equal and the absolute ROCD between waypoints is within ± 500
 144 feet per minute (indicative of shallow climb/descent) (Dalmau and Prats, 2017), we assume
 145 that the aircraft performs: (i) a step climb (descent) at the start (end) of the segment when $dt \leq$
 146 0.5 h; or (ii) a step climb/descent at the mid-point when the segment length is large, identified
 147 when $dt > 0.5$ h. When the difference in altitude is large (absolute ROCD > 500 feet per minute)
 148 (Dalmau and Prats, 2017), we use a linear interpolation to represent a continuous climb/descent

149 between the recorded waypoints. In rare instances where the altitude between two waypoints
150 is below 50% of the service ceiling altitude for long time periods ($dt > 1$ h), i.e., no information
151 is available during the cruise phase of flight, we assume that the aircraft will climb and cruise
152 at ~80% of the service ceiling altitude that is rounded to the nearest flight level, and then
153 descent to the next recorded waypoint. We note that the incorporation of step climbs/descents
154 at cruise altitudes is necessary to ensure that the interpolated trajectories conform to the
155 airspace design and air traffic management constraints in the real-world (Dalmau and Prats,
156 2017) (Fig. S5). The availability of satellite ADS-B coverage also improves the accuracy of
157 the lateral and vertical profile of the interpolated flight trajectories (Fig. S6a). We note that the
158 temporal resolution between waypoints that is provided by the ADS-B dataset (~300 s) might
159 not be sufficient in capturing the full flight trajectory in the Terminal Radar Approach Control
160 (TRACON), especially when flights are in a holding pattern, and the great-circle interpolation
161 between recorded waypoints would likely underestimate the flight distance flown during the
162 landing and take-off (LTO) phase of flight.



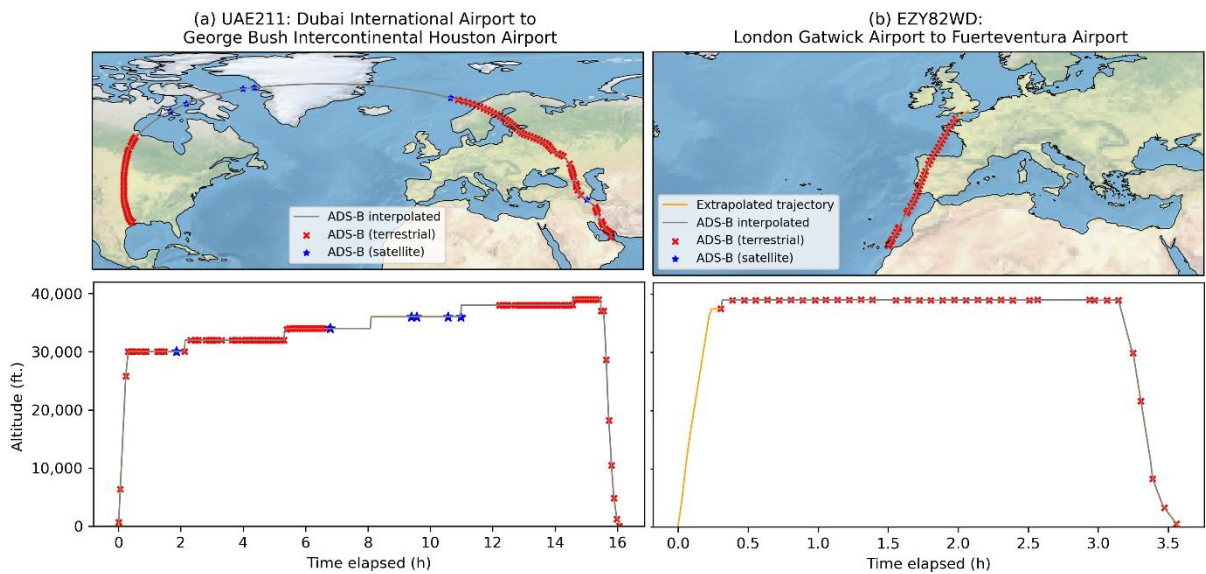
163
164 **Figure S5: Vertical profile of the interpolated trajectories from 50 unique flights selected at random, where**
165 **each line represents the trajectory of one unique flight.**

166 Fig. S5 also shows that the trajectories for a subset of flights are incomplete, where the first
167 waypoint does not start at the origin airport, and/or the final waypoint does not end at the
168 destination airport. Whenever possible, we complete the flight trajectories using one of the two
169 approaches: (i) a great-circle path is used to extrapolate the flight trajectory from the origin
170 (destination) airport to the first (final) waypoint if the airport metadata is provided by the ADS-
171 B dataset; and (ii) if airport data is not available and the first/final waypoint is below 10,000
172 feet, we assign and extrapolate the flight trajectory to the nearest airport. Fig. S6b provides an
173 example where the missing flight segment from the origin airport to the first recorded waypoint
174 is completed when the airport metadata is available.

175 Additional quality checks are then performed on each of the completed flight trajectory to
176 ensure its validity:

- 177 1. the total length of the extrapolated flight segments, i.e., distance from the origin airport
178 to first waypoint plus the final waypoint to destination airport, must be less than 90%
179 of the distance between airports, and
- 180 2. if the first (final) waypoint is below 50% of the service ceiling altitude, the duration of
181 the extrapolated flight segments from the origin airport (final waypoint) to the first
182 waypoint (destination airport) must be less than 0.5 h,
- 183 3. the completed flight trajectory must have a realistic flight time (up to 20 h). For each
184 flight, the maximum flight time is estimated by assuming that the aircraft operates at a
185 mean speed of 200 m s^{-1} ($\sim 700 \text{ km h}^{-1}$) for jet aircraft and 70 m s^{-1} ($\sim 250 \text{ km h}^{-1}$) for
186 turboprops and piston aircraft, and multiplied by a tolerance factor of between 1.2
187 (long-haul flights) and 2.5 (short-haul) depending on the time difference between the
188 first and final recorded waypoint, and

189 4. the segment length between successive waypoints must be realistic. The maximum
 190 segment length between waypoints is estimated by multiplying dt with an assumed
 191 mean speed (200 m s^{-1} or $\sim 700 \text{ km h}^{-1}$ for jet aircraft, and 70 m s^{-1} $\sim 250 \text{ km h}^{-1}$ for
 192 turboprops and piston aircraft), and a tolerance factor of 2 is added.



193
 194 **Figure S6: The interpolated lateral (top) and vertical (bottom) trajectory from two example flights.**
 195 **Basemap plotted using Cartopy 0.21.1 © Natural Earth; license: public domain.**

196 Flights that violate Condition (2) are likely caused by upstream errors in linking the call sign
 197 and flight schedule database to obtain the airport metadata, and we replace the flight trajectory
 198 by assuming a great-circle path between the given origin-destination airports (1.5% of all
 199 flights). Flights that violate Conditions (1), (3) and/or (4) are generally indicative of the
 200 trajectory containing erroneous waypoints and are rejected.

201 S1.3 Summary statistics & validation

202 Fig. S7 presents the summary statistics for the cleaned ADS-B dataset and shows that:

- 203 • 103.7 million flight trajectories are recorded between 2019 and 2021 (Fig. S7a),
- 204 • 75% of all flights are carried out by jet aircraft, 9% by turboprops, and the remaining
 205 15% by piston aircraft (Fig. S7b),

- 206 • origin and destination airport metadata are available for 79% of all flights, and this
- 207 figure increases to 91% when piston aircraft, mostly used in general aviation, are
- 208 excluded (Fig. S7c),
- 209 • 67% of all flights have full trajectory coverage, i.e., first waypoint starting from the
- 210 origin airport and ending at the destination airport, and this figure increases to 78%
- 211 when piston aircraft are excluded (Fig. S7d),
- 212 • 5.0% of all flights are rejected from the ADS-B dataset (Fig. S7e), and
- 213 • at the waypoint level, 99% of the recorded ADS-B signals are from terrestrial receivers
- 214 and the remaining 1% are provided by satellite receivers (Fig. S7f).

215 The 5% of all flights that are rejected from the ADS-B dataset are caused by identified errors
 216 in their respective flight trajectories, for example,

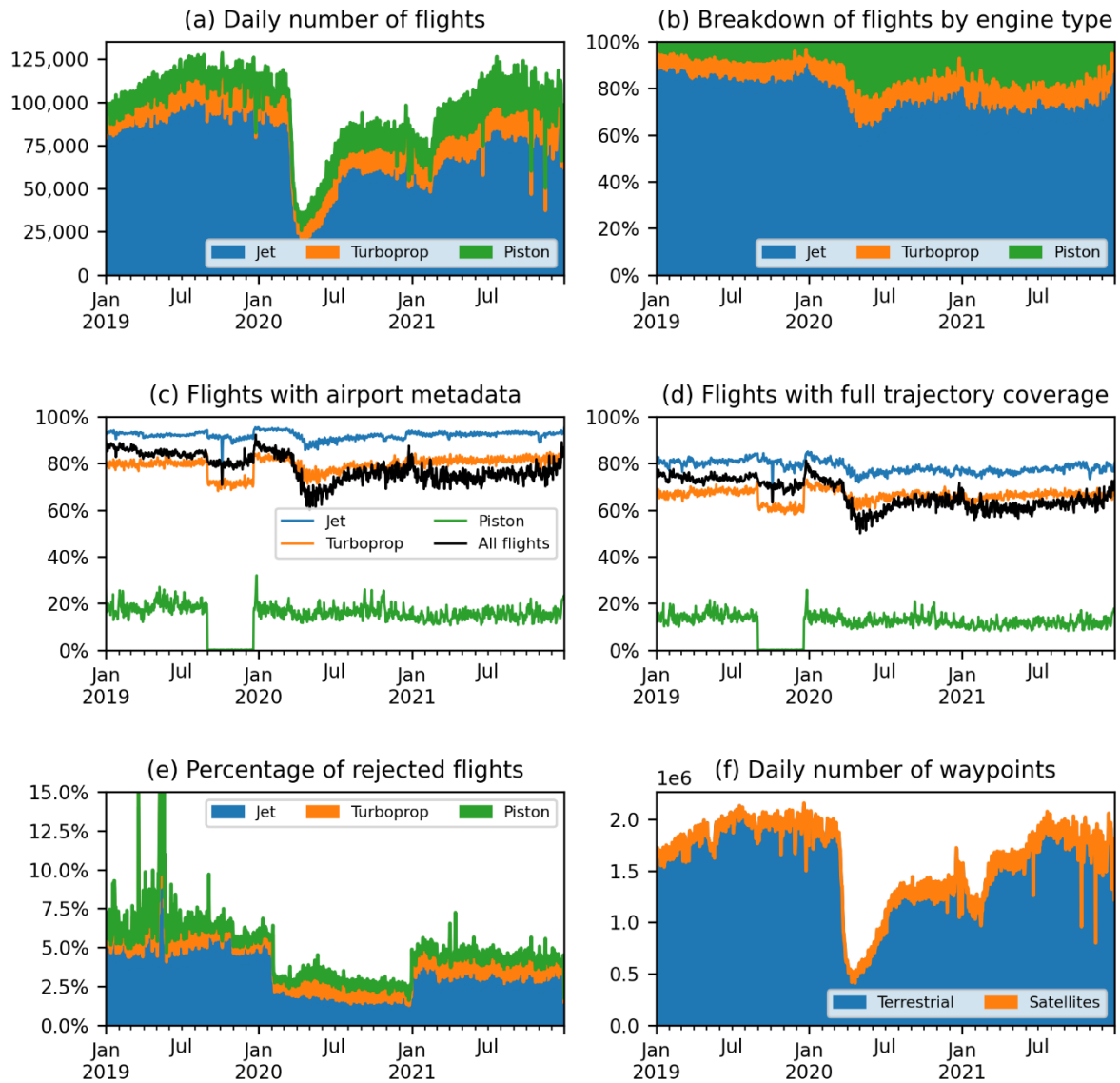
- 217 • trajectories that contain less than three waypoints (57% of all rejected flights),
- 218 • trajectories with very long extrapolated segment lengths, i.e., > 90% of the distance
- 219 between the origin-destination airport (21% of all rejected flights),
- 220 • flights with unrealistic flight time (13% of all rejected flights), and
- 221 • flight segments with unrealistic ground speed (5% of all rejected flights).

222 **Table S1: Comparison of the global annual number of flights from the cleaned ADS-B dataset versus**
 223 **statistics published by ICAO and IATA.**

| | ADS-B dataset: Total number of flights (millions) | | ICAO & IATA: Number of departures from scheduled services (million) | Difference ^a |
|-------------|--|-------------------|---|-------------------------|
| | All flights | Jet and turboprop | | |
| 2019 | 40.2 | 36.5 | 38.3 | -4.7% |
| 2020 | 27.9 | 23.0 | 20.3 | +13.3% |
| 2021 | 35.6 | 28.2 | 24.1 ^b | +17.0% |

224 ^a: Difference in the total number of jet and turboprop flights in the ADS-B dataset relative to ICAO & IATA.

225 ^b: Extrapolated using preliminary statistics published by IATA (2022).



226

227

228

229

230

Figure S7: Summary statistics of the cleaned ADS-B dataset, showing the (a) daily number of flights globally; (b) breakdown of flights by engine type; (c) percentage of flights with origin-destination airport metadata; (d) percentage of flights with full trajectory coverage; (e) percentage of rejected flights due to unrealistic flight time and/or segment length; and (f) daily number of waypoints.

231

To assess the completeness of the processed ADS-B dataset, we compared the: (i) global annual

232

number of flights with statistics published by ICAO and IATA (ICAO 2019, 2021b, 2022;

233

IATA, 2022), which counts the number of departures from scheduled flights; and (ii) global

234

annual flight distance flown with estimates provided by Airlines for America (2022), which

235

captures the air traffic activity from passenger and cargo airline operations. As these datasets

236

only include the air traffic activity from scheduled/commercial flights, we only include flights

237

that are performed by jet and turboprop aircraft in the ADS-B dataset. Flights that arise from

238 general aviation, which are identified by those performed by piston aircraft, are excluded from
 239 the comparison.

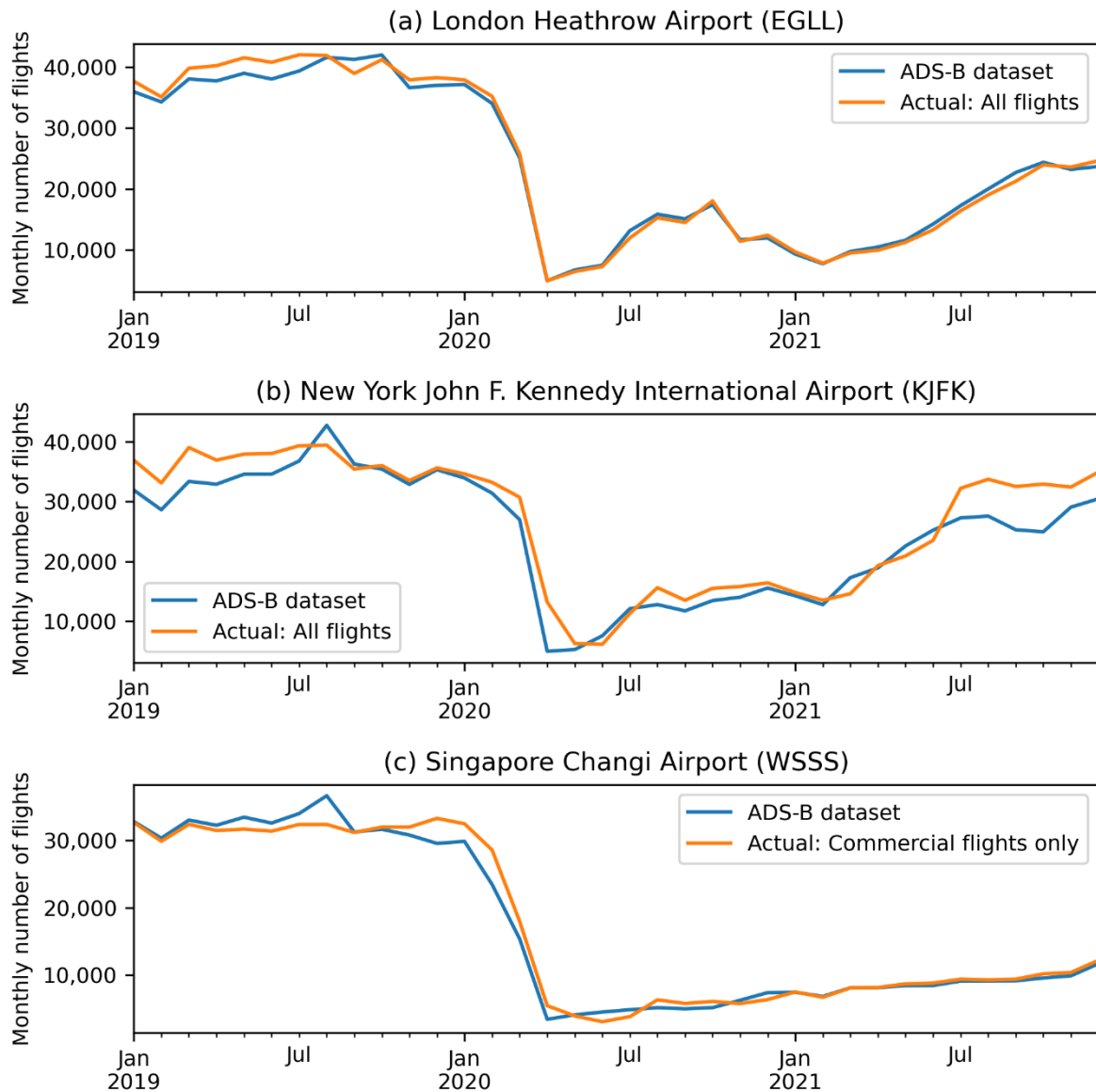
240 **Table S2: Comparison of the global annual flight distance flown that is derived from the cleaned ADS-B**
 241 **dataset versus estimates from produced by Airlines for America.**

| | Total flight distance flown (x10 ⁹ km) | | | Difference |
|-------------|---|--------------------------|----------------------|------------|
| | ADS-B: All flights | ADS-B: Jet and turboprop | Airlines for America | |
| 2019 | 60.9 | 60.3 | 56.2 | +8.4% |
| 2020 | 34.5 | 33.7 | 28.0 | +23.2% |
| 2021 | 41.9 | 40.8 | 33.7 | +24.3% |

242 ^a: Difference in the total flight distance flown from jet and turboprop flights in the ADS-B dataset relative to
 243 Airlines for America (2022).

244 The comparison with statistics from ICAO and IATA (Table S1) shows that the number of jet
 245 and turboprop flights captured by the ADS-B dataset in 2019 (36.5 million) is ~4.7% lower
 246 than the global statistics (38.3 million), and this is likely caused by: (i) the smaller global
 247 coverage area of ADS-B receiver networks in 2019 relative to 2021 (Fig. S1), where the subset
 248 of flights outside the coverage area might not be recorded; and (ii) of the presence of erroneous
 249 trajectories in the raw ADS-B dataset in 2019, where 6.6% of flights being rejected because
 250 the validity of their trajectories cannot be verified (Fig. S7e). The ADS-B dataset captured a
 251 higher number of jet and turboprop flights relative to the ICAO and IATA statistics in 2020
 252 (23.0 vs. 20.3 million, +13%) and 2021 (28.2 vs. 24.1 million, +17%), and these discrepancies
 253 could be due to the change in the proportion of unscheduled flights, i.e., charter flights, cargo
 254 services and private aviation, which increased from 4.1% in 2019 to 7.5% in 2020 (Sobieralski
 255 and Mumbower, 2022; ICAO, 2021b). Notably, the global annual flight distance flown from
 256 jet and turboprop aircraft in the ADS-B dataset are around 8–24 % higher when compared to
 257 estimates produced by Airlines for America (Table S2), and this could be because Airlines for
 258 America: (i) only accounts for the flight distance flown from passenger and cargo airline
 259 operations; and (ii) estimated the flight distance flown based on scheduled activity and likely

260 assumed a great-circle path between the origin-destination airport with a lateral inefficiency
261 factor.



262
263 **Figure S8: Comparison of the monthly number of air traffic movements derived from the ADS-B dataset**
264 **relative to published traffic statistics from: (a) London Heathrow Airport; (b) New York John F. Kennedy**
265 **International Airport; and (c) Singapore Changi Airport.**

266 In addition to the global statistics, we also compared the number of air traffic movements
267 derived from the ADS-B dataset with official traffic statistics published by London Heathrow
268 Airport (ICAO airport code: EGLL) (Heathrow Airport, 2022b), New York John F. Kennedy
269 International Airport (KJFK) (Port Authority of New York and New Jersey, 2022), and

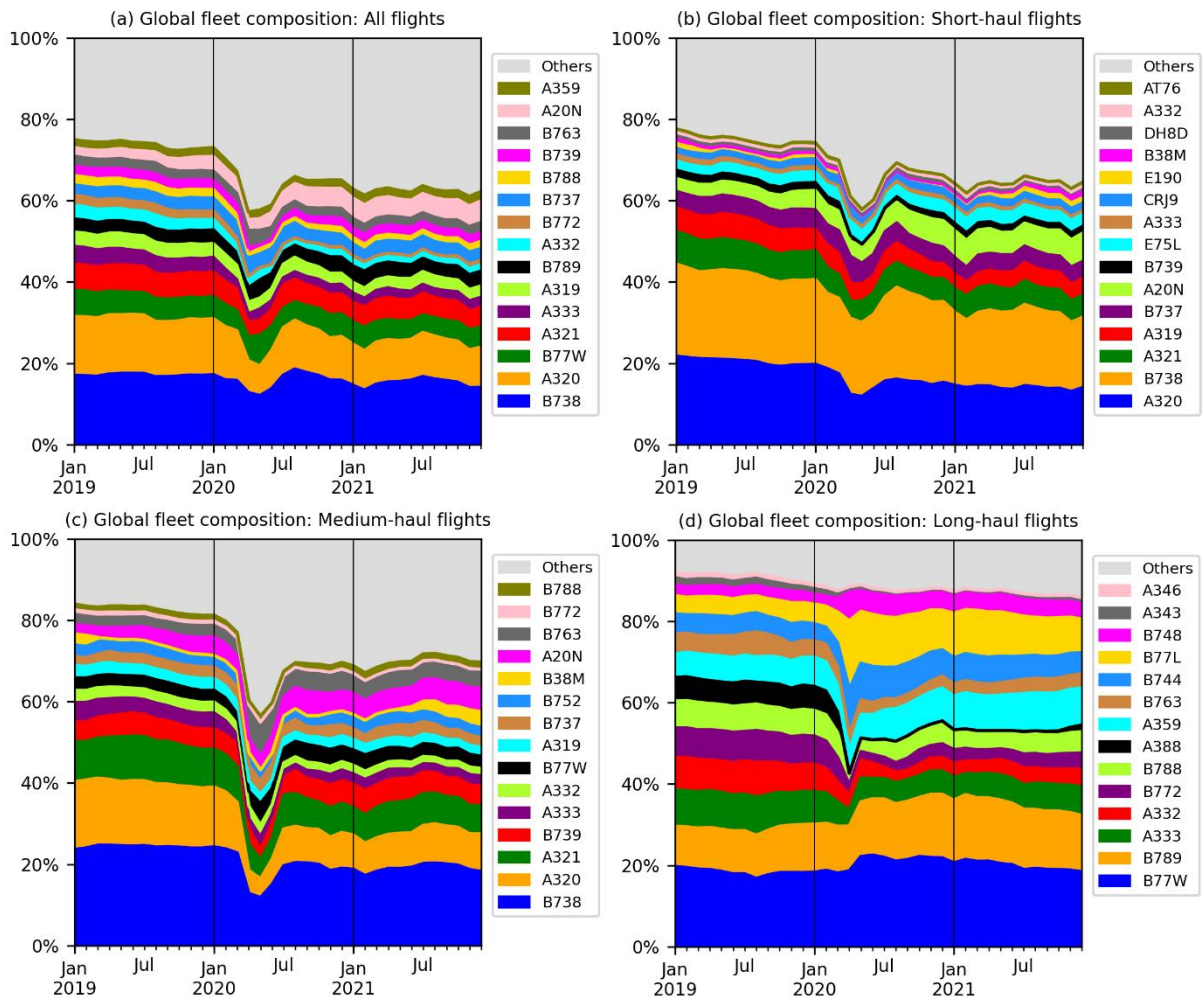
270 Singapore Changi Airport (WSSS) (Changi Airport Group, 2022a, 2022b). Fig. S8 shows that
271 the total number of aircraft movements derived from the processed ADS-B dataset can be
272 between 1–8% lower when compared with published statistics from the three airports (-1.3%
273 for EGLL, -8.1% for KJFK and -1.3% for WSSS between 2019 and 2021). For the comparison
274 with WSSS, we note that the published data does not include air traffic movements from freight
275 operations and private aviation, and therefore, the number of flights in the ADS-B dataset can
276 be higher than the published statistics.

277 **S2 Aircraft-engine combination**

278 Fig. S9 provides a breakdown of the 2019–2021 global fleet composition in the ADS-B dataset
279 by their ICAO aircraft type designator. We note that the same ICAO aircraft type designator
280 can consist of multiple aircraft variants that are powered by different engine types. For
281 example, the “A320” ICAO aircraft type designator covers the A320-212, A320-214, A320-
282 231, and A320-232 variants, and these variants can either be powered by the IAE V2500 or
283 CFM56-5 engine series. The aircraft variant is used by the Base of Aircraft Data Family 4
284 (BADA 4) aircraft performance model to simulate the fuel consumption (EUROCONTROL,
285 2016), while the specific engine model is required by the ICAO Aircraft Engine Emissions
286 Databank (EDB) (EASA, 2021) to estimate the emission indices (EI) of nitrogen oxide (NO_x),
287 carbon monoxide (CO), unburnt hydrocarbons (HC) and non-volatile particulate matter
288 (nvPM) for each flight.

289 To obtain this information, we utilise a global fleet database from a commercial company
290 (Cirium) to link the registered aircraft tail number to the specific aircraft variant and engine
291 model (Cirium, 2022). The fleet database covers around 59% of all flights in the ADS-B dataset
292 or 79% of all flights that are carried out by jet aircraft. Table S3 provides a breakdown of
293 engine market share for the commonly used passenger aircraft types for flights that are covered

294 by the fleet database. For the remaining flights not covered by fleet database, we assign the
 295 default aircraft-engine combination using the Base of Aircraft Data (BADA) database (Table
 296 S4) with modifications applied to the A320 (replaced V2500-A1 with CFM56-5B4), B788
 297 (Trent 1000-A → GEnX-1B70/P2) and B789 (Trent 1000-J → GEnX-1B75/P2) to use the
 298 engine type with the highest market share (shown in Table S3).



299

300 **Figure S9: Global fleet composition by distance travelled for: (a) all flights; (b) short-haul flights ($t \leq 3$ h);**
 301 **(c) medium-haul flights ($3 < t < 6$ h); and (d) long-haul flights ($t > 6$ h) in the ADS-B dataset between 2019**
 302 **and 2021.**

303 **Table S3: Breakdown of the engine market share for 23 commonly used passenger aircraft types in the**
 304 **ADS-B dataset by flight distance travelled. Flights are only included in this analysis if the registered aircraft**
 305 **tail number is available in the fleet database.**

| ICAO aircraft type designator | Engine Name | Engine UID - ICAO EDB | Market share (%) | | |
|-------------------------------|--------------------------|-----------------------|------------------|------|------|
| | | | 2019 | 2020 | 2021 |
| A319 | CFM56-5B5/3 | 01P08CM106 | 30% | 21% | 21% |
| | CFM56-5B6/3 | 01P08CM107 | 25% | 23% | 23% |
| | CFM56-5B7/3 | 01P08CM108 | 9% | 18% | 17% |
| | V2522-A5 | 01P10IA019 | 11% | 10% | 8% |
| | V2524-A5 | 01P10IA020 | 22% | 22% | 25% |
| | V2527-A5M | 01P10IA023 | 4% | 7% | 6% |
| A320 | CFM56-5B4/3 | 01P08CM105 | 52% | 55% | 56% |
| | CFM56-5B6/3 | 01P08CM107 | 7% | 4% | 3% |
| | V2527-A5 | 01P10IA021 | 38% | 38% | 38% |
| | V2527-A5E | 01P10IA022 | 3% | 3% | 4% |
| A321 | CFM56-5B1/3 | 01P08CM102 | 2% | 1% | 1% |
| | CFM56-5B2/3 | 01P08CM103 | 2% | 3% | 3% |
| | CFM56-5B3/3 | 01P08CM104 | 33% | 35% | 37% |
| | V2530-A5 | 01P10IA024 | 3% | 2% | 2% |
| | V2533-A5 | 01P10IA025 | 60% | 58% | 57% |
| A19N | LEAP-1A26CJ | 01P20CM129 | 100% | 100% | 100% |
| A20N | LEAP-1A26/26E1 | 01P20CM128 | 59% | 55% | 53% |
| | PW1127G-JM | 01P18PW153 | 39% | 43% | 46% |
| | PW1127GA-JM | 01P18PW152 | 2% | 2% | 2% |
| A21N | LEAP-1A35A/33/33B2/32/30 | 01P20CM132 | 40% | 39% | 43% |
| | PW1130G-JM | 01P18PW155 | 7% | 7% | 3% |
| | PW1133GA-JM | 01P18PW156 | 2% | 4% | 7% |
| | PW1133G-JM | 01P18PW157 | 51% | 51% | 48% |
| A332 | Trent 772 | 01P14RR102 | 100% | 100% | 100% |
| A333 | Trent 768 | 01P14RR101 | 4% | 3% | 5% |
| | Trent 772 | 01P14RR102 | 96% | 97% | 95% |
| A346 | Trent7000-72 | 02P23RR141 | 93% | 100% | 0% |
| | CFM56-5B6/3 | 01P08CM107 | 7% | 0% | 0% |
| A359 | Trent XWB-75 | 01P18RR121 | 3% | 5% | 8% |
| | Trent XWB-84 | 01P18RR124 | 97% | 95% | 92% |
| A35K | Trent XWB-97 | 01P21RR125 | 100% | 100% | 100% |
| A388 | Trent 970-84 | 01P18RR103 | 67% | 56% | 18% |
| | Trent 972-84 | 01P18RR104 | 12% | 12% | 0% |
| | Trent 972E-84 | 01P18RR105 | 22% | 33% | 82% |
| B737 | CFM56-7B20E | 01P11CM111 | 9% | 8% | 8% |
| | CFM56-7B22E | 01P11CM112 | 65% | 67% | 68% |
| | CFM56-7B24E | 01P11CM114 | 23% | 23% | 22% |
| | CFM56-7B26E | 01P11CM116 | 3% | 3% | 2% |

306

| ICAO aircraft type designator | Engine Name | Engine UID - ICAO EDB | Market share (%) | | |
|-------------------------------|-----------------|-----------------------|------------------|------|------|
| | | | 2019 | 2020 | 2021 |
| B738 | CFM56-7B24E | 01P11CM114 | 16% | 18% | 17% |
| | CFM56-7B26E | 01P11CM116 | 73% | 71% | 72% |
| | CFM56-7B27E | 01P11CM121 | 8% | 8% | 8% |
| | CFM56-7B27E/B1 | 01P11CM122 | 3% | 2% | 2% |
| B739 | CFM56-7B24E | 01P11CM114 | 3% | 2% | 3% |
| | CFM56-7B26E | 01P11CM116 | 50% | 47% | 42% |
| | CFM56-7B27E | 01P11CM121 | 45% | 49% | 54% |
| | CFM56-7B27E/F | 01P11CM125 | 2% | 2% | 2% |
| B744 | CF6-80C2B1F | 01P02GE186 | 76% | 70% | 68% |
| | CF6-80C2B5F | 01P03GE187 | 24% | 30% | 32% |
| B762 | CF6-80C2B5F | 01P03GE187 | 23% | 5% | 7% |
| | CF6-80C2B6F | 01P02GE188 | 77% | 95% | 93% |
| B763 | CF6-80C2B6F | 01P02GE188 | 100% | 100% | 100% |
| B77L | GE90-110B1 | 01P21GE216 | 90% | 95% | 94% |
| | GE90-115B | 01P21GE217 | 10% | 5% | 6% |
| B77W | GE90-115B | 01P21GE217 | 100% | 100% | 100% |
| B788 | GEnx-1B64/P2 | 01P17GE206 | 16% | 13% | 8% |
| | GEnx-1B67/P2 | 01P17GE207 | 11% | 10% | 10% |
| | GEnx-1B70/75/P2 | 01P17GE209 | 15% | 17% | 19% |
| | GEnx-1B70/P2 | 01P17GE210 | 27% | 31% | 37% |
| | Trent 1000-AE3 | 02P23RR126 | 2% | 3% | 2% |
| | Trent 1000-CE3 | 02P23RR127 | 7% | 4% | 2% |
| | Trent 1000-D3 | 02P23RR128 | 4% | 4% | 6% |
| | Trent 1000-G3 | 02P23RR129 | 18% | 17% | 16% |
| B789 | GEnx-1B74/75/P2 | 01P17GE211 | 58% | 60% | 63% |
| | GEnx-1B76A/P2 | 01P17GE214 | 4% | 6% | 5% |
| | Trent 1000-J3 | 02P23RR131 | 34% | 30% | 27% |
| | Trent 1000-K3 | 02P23RR132 | 4% | 4% | 4% |
| B78X | GEnx-1B74/75/P2 | 01P17GE211 | 22% | 23% | 26% |
| | GEnx-1B76/P2 | 01P17GE213 | 31% | 47% | 43% |
| | GEnx-1B76A/P2 | 01P17GE214 | 6% | 5% | 3% |
| | Trent 1000-M3 | 02P23RR134 | 41% | 25% | 27% |

307

308

309

310

311

312 **Table S4: Default aircraft-engine assignment for jet aircraft if the registered aircraft tail number is not**
 313 **included in the fleet database. For turboprop and piston aircraft, their respective engines are not available**
 314 **in the ICAO EDB and a constant emissions index is used to calculate the NO_x, CO, HC and nvPM emissions.**

| ICAO Aircraft Code | Engine - EDB | Engine UID - EDB | ICAO Aircraft Code | Engine - EDB | Engine UID - EDB |
|--------------------|--------------------------|------------------|--------------------|-----------------------|------------------|
| A148 | D-436-148 | 13ZM003 | C650 | TFE731-3 | 1AS002 |
| A158 | D-436-148 | 13ZM003 | C680 | PW306B | 7PW078 |
| A20N | PW1127G-JM | 01P22PW163 | C750 | AE3007C | 6AL022 |
| A21N | LEAP-1A35A/33/33B2/32/30 | 01P20CM132 | CL30 | HTF7000 (AS907-1-1A) | 11HN003 |
| A306 | PW4158 | 1PW048 | CL60 | CF34-3B | 01P05GE189 |
| A30B | CF6-50C2 | 3GE074 | CRJ1 | CF34-3A1 | 1GE035 |
| A310 | CF6-80C2A2 | 1GE015 | CRJ2 | CF34-3B1 | 01P05GE189 |
| A318 | CFM56-5B9 | 01P08CM110 | CRJ9 | CF34-8C5 | 01P08GE190 |
| A319 | V2522-A5 | 01P10IA019 | CRJX | CF34-8C5A1 | 01P08GE191 |
| A320 | CFM56-5B4/3 | 01P08CM105 | DC10 | CF6-50C2 | 3GE074 |
| A321 | V2530-A5 | 01P10IA024 | DC87 | CFM56-2-C5 | 1CM003 |
| A332 | Trent 772B | 01P14RR102 | DC93 | JT8D-11 | 1PW008 |
| A333 | Trent 768 | 01P14RR101 | DC94 | JT8D-11 | 1PW008 |
| A339 | Trent7000-72 | 02P23RR141 | E135 | AE3007A1/3 | 01P06AL030 |
| A342 | CFM56-5C4 | 2CM015 | E145 | AE3007A1 | 01P06AL028 |
| A343 | CFM56-5C4 | 2CM015 | E170 | CF34-8E5 | 01P08GE197 |
| A345 | Trent 553 | 8RR044 | E190 | CF34-10E6 | 8GE116 |
| A346 | Trent 556 | 6RR041 | E195 | CF34-10E7 | 8GE119 |
| A359 | Trent XWB-84 | 01P18RR124 | E290 | PW1919G | 20PW134 |
| A35K | Trent XWB-97 | 01P21RR125 | E35L | AE 3007A1E | 01P06AL032 |
| A388 | Trent 970-84 | 01P18RR103 | E45X | AE 3007A1E | 01P06AL032 |
| A3ST | CF6-80C2A8 | 1GE021 | E545 | AS907-3-1E | 01P14HN014 |
| B38M | LEAP-1B27 | 01P20CM136 | E550 | AS907-3-1E | 01P14HN015 |
| B39M | LEAP-1B28 | 01P20CM140 | E75L | CF34-8E5A1 | 01P08GE191 |
| B462 | ALF 502R-5 | 1TL003 | E75S | CF34-8E5A1 | 01P08GE191 |
| B463 | ALF 502R-5 | 1TL003 | F100 | TAY Mk620-15 | 1RR020 |
| B703 | JT3D-3B | 1PW001 | F28 | Spey 555 | 4RR035 |
| B712 | BR700-715A1-30 | 4BR002 | F2TH | PW308C BS 1289 | 03P14PW194 |
| B722 | JT8D-15 | 1PW009 | F70 | TAY Mk620-15 | 1RR020 |
| B732 | JT8D-15 | 1PW009 | F900 | TFE731-2-2B | 1AS001 |
| B733 | CFM56-3B2 | 1CM005 | FA10 | TFE731-2-2B | 1AS001 |
| B734 | CFM56-5A | 1CM008 | FA50 | TFE731-2-2B | 1AS001 |
| B735 | CFM56-3 | 1CM004 | FA7X | PW307A | 03P16PW192 |
| B736 | CFM56-7B22E | 01P11CM112 | G150 | TFE731-2-2B | 1AS001 |
| B737 | CFM56-7B24E | 01P11CM114 | G280 | AS907-2-1G (HTF7250G) | 01P11HN012 |
| B738 | CFM56-7B26E | 01P11CM116 | GL5T | BR700-710A2-20 | 01P04BR013 |
| B739 | CFM56-7B27E | 01P11CM121 | GLEX | BR700-710A2-20 | 01P04BR013 |

315

316

| ICAO Aircraft Code | Engine - EDB | Engine UID - EDB | ICAO Aircraft Code | Engine - EDB | Engine UID - EDB |
|--------------------|-------------------|------------------|--------------------|------------------|------------------|
| B742 | RB211-524D4 | 1RR008 | GLF2 | SPEY Mk511 | 8RR043 |
| B743 | JT9D-7R4G2 | 1PW029 | GLF5 | BR700-710C4-11 | 01P06BR014 |
| B744 | CF6-80C2B1F | 01P02GE186 | H25B | TFE731-3 | 1AS002 |
| B748 | GEnx-2B67 | 01P17GE215 | HA4T | PW308A | 01P07PW145 |
| B752 | RB211-535E4 | 1RR013 | IL76 | D-30KP-2 | 1AA002 |
| B753 | RB211-535E4-B | 3RR028 | IL86 | NK-86 | 1KK003 |
| B762 | CF6-80A2 | 1GE012 | IL96 | PS-90A | 1AA005 |
| B763 | PW4060 | 1PW043 | L101 | RB211-22B | 1RR002 |
| B764 | CF6-80C2B6F | 01P02GE188 | LJ35 | TFE731-2-2B | 1AS001 |
| B772 | Trent 892 | 2RR027 | LJ45 | TFE731-2-2B | 1AS001 |
| B773 | Trent 892 | 2RR027 | LJ60 | PW306A | 7PW077 |
| B77L | GE90-110B1 | 01P21GE216 | MD11 | PW4460 | 1PW052 |
| B77W | GE90-115B | 01P21GE217 | MD82 | JT8D-217C | 4PW070 |
| B788 | GEnx-1B70/P2 | 01P17GE210 | MD83 | JT8D-219 | 1PW019 |
| B789 | GEnx-1B75/P2 | 01P17GE212 | Q4 | AE 3007H | 8AL025 |
| B78X | GEnx-1B76/P2 | 01P17GE213 | RJ1H | LF507-1F, -1H | 1TL004 |
| BA11 | SPEY Mk511 | 8RR043 | RJ85 | LF507-1F, -1H | 1TL004 |
| BE40 | JT15D-5C | 1PW038 | SU95 | SaM146-1S17 | 01P11PJ003 |
| BER2 | D-436-148 F1 | 13ZM004 | T134 | D-30 (II series) | 1AA001 |
| C550 | JT15D-4 series | 1PW036 | T154 | D-30KU-154 | 1AA004 |
| C551 | JT15D-4 series | 1PW036 | T204 | PS-90A | 1AA005 |
| C560 | JT15D-5, -5A, -5B | 1PW037 | YK42 | D-36 | 1ZM001 |

317

318 **S3 Passenger Load Factor**

319 The passenger load factor, i.e., the number of passengers divided by the aircraft seat capacity,
320 is required to estimate the aircraft mass, c.f. Eq. (1) in the main text, which is subsequently
321 used by BADA to estimate the thrust force and fuel consumption rate. Existing studies
322 generally: (i) use a constant annual passenger load factor globally (Quadros et al., 2022;
323 Wasiuk et al., 2015); or (ii) assume a nominal (reference) mass for a given aircraft type (Teoh
324 et al., 2022a) that is provided by the BADA database (EUROCONTROL, 2019, 2016).
325 However, the COVID-19 pandemic led to significant temporal and regional variations in the
326 passenger load factor that needs to be accounted for (ICAO, 2022).

327 Here, we compile the global (monthly) and regional (annual) passenger load factor (LF)
328 statistics between December-2018 and January-2022 from published data by ICAO and IATA

329 (ICAO 2019, 2021b; 2022; IATA, 2022) (Tables S5 and S6). As a breakdown of the monthly
 330 regional passenger LF is not available, we approximate it as a ratio of the regional and global
 331 annual LF,

$$\text{Regional LF}_{\text{month}} = \left(\frac{\text{Regional LF}_{\text{annual}}}{\text{Global LF}_{\text{annual}}} \right) \times \text{Global LF}_{\text{month}}. \quad (\text{S1})$$

332 A linear interpolation relative to the monthly regional LF is then used to obtain the daily
 333 regional LF, and this approach ensures that the day-to-day passenger LF is continuous without
 334 abrupt shifts in magnitude (Fig. S10). For each flight, we assign the: (i) regional passenger LF
 335 that is based on the region of the origin airport that is identified using the first letter of the
 336 ICAO airport code (Table S7); or (ii) global mean passenger LF if airport data is not available.
 337 In real-world operations, the passenger/weight LF varies between different airlines (low-cost
 338 vs. full-service carriers), aircraft type (narrowbody vs. widebody aircraft) and mission profile
 339 (short-haul vs. long haul flights, and passenger vs. freight services). However, our approach is
 340 unable to account for these LF variabilities because of the lack of publicly available
 341 disaggregated LF data.

342 **Table S5: Annual available seat kilometre (ASK) and passenger load factor between 2019 and 2021.**

| Region | ASK (% of global) | | | Passenger Load Factor (%) | | |
|-----------------------------|-------------------|------|------|---------------------------|------|------|
| | 2019 | 2020 | 2021 | 2019 | 2020 | 2021 |
| Global | 100 | 100 | 100 | 82.4 | 65.3 | 67.9 |
| Europe | 26.0 | 22.5 | 24.9 | 85.0 | 68.1 | 68.6 |
| Africa | 2.4 | 2.1 | 1.9 | 72.4 | 60.8 | 59.5 |
| Middle East | 9.9 | 9.4 | 6.5 | 75.6 | 59.9 | 51.5 |
| Asia and Pacific | 35.1 | 36.6 | 27.5 | 81.7 | 67.8 | 62.6 |
| North America | 21.6 | 24.6 | 32.6 | 84.8 | 59.6 | 73.8 |
| Latin America and Caribbean | 5.0 | 4.8 | 6.6 | 82.1 | 74.8 | 77.3 |

343

344

345
346

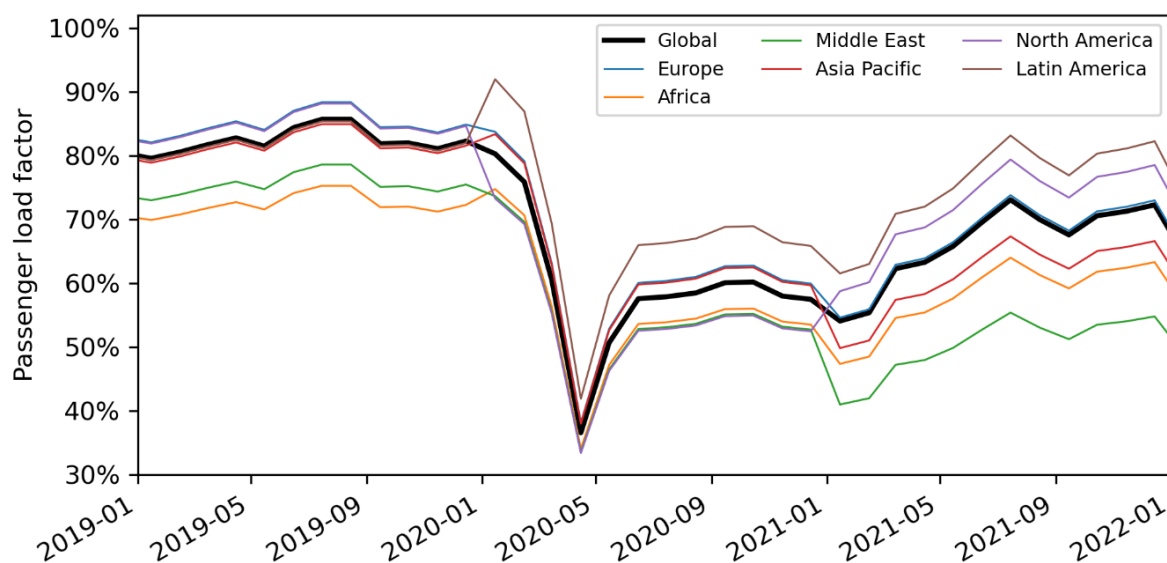
Table S6: Actual monthly global passenger load factor compiled using published data from ICAO (2022), and the monthly regional passenger load factor is estimated using Eq. (S1).

| Month | Passenger Load Factor (%) | | | | | | |
|----------|---------------------------|--------|--------|-------------|----------------|---------------|---------------------------|
| | Global | Europe | Africa | Middle East | Asia & Pacific | North America | Latin America & Caribbean |
| Dec-2018 | 80.4 | 82.9 | 70.6 | 73.7 | 79.7 | 82.7 | 80.1 |
| Jan-2019 | 79.6 | 82.1 | 69.9 | 73.0 | 78.9 | 81.9 | 79.3 |
| Feb-2019 | 80.6 | 83.1 | 70.8 | 73.9 | 79.9 | 82.9 | 80.3 |
| Mar-2019 | 81.7 | 84.3 | 71.8 | 74.9 | 81.0 | 84.1 | 81.4 |
| Apr-2019 | 82.8 | 85.4 | 72.7 | 75.9 | 82.1 | 85.2 | 82.5 |
| May-2019 | 81.5 | 84.1 | 71.6 | 74.8 | 80.8 | 83.9 | 81.2 |
| Jun-2019 | 84.4 | 87.0 | 74.1 | 77.4 | 83.7 | 86.8 | 84.1 |
| Jul-2019 | 85.7 | 88.4 | 75.3 | 78.6 | 85.0 | 88.2 | 85.4 |
| Aug-2019 | 85.7 | 88.4 | 75.3 | 78.6 | 85.0 | 88.2 | 85.4 |
| Sep-2019 | 81.9 | 84.5 | 71.9 | 75.1 | 81.2 | 84.3 | 81.6 |
| Oct-2019 | 82.0 | 84.6 | 72.0 | 75.2 | 81.3 | 84.4 | 81.7 |
| Nov-2019 | 81.1 | 83.6 | 71.2 | 74.4 | 80.4 | 83.4 | 80.8 |
| Dec-2019 | 82.3 | 84.9 | 72.3 | 75.5 | 81.6 | 84.7 | 82.0 |
| Jan-2020 | 80.3 | 83.7 | 74.8 | 73.7 | 83.4 | 73.3 | 92.0 |
| Feb-2020 | 75.9 | 79.2 | 70.7 | 69.6 | 78.8 | 69.3 | 86.9 |
| Mar-2020 | 60.6 | 63.2 | 56.4 | 55.6 | 62.9 | 55.3 | 69.4 |
| Apr-2020 | 36.6 | 38.2 | 34.1 | 33.6 | 38.0 | 33.4 | 41.9 |
| May-2020 | 50.7 | 52.9 | 47.2 | 46.5 | 52.6 | 46.3 | 58.1 |
| Jun-2020 | 57.6 | 60.1 | 53.6 | 52.8 | 59.8 | 52.6 | 66.0 |
| Jul-2020 | 57.9 | 60.4 | 53.9 | 53.1 | 60.1 | 52.8 | 66.3 |
| Aug-2020 | 58.5 | 61.0 | 54.5 | 53.7 | 60.7 | 53.4 | 67.0 |
| Sep-2020 | 60.1 | 62.7 | 56.0 | 55.1 | 62.4 | 54.9 | 68.8 |
| Oct-2020 | 60.2 | 62.8 | 56.1 | 55.2 | 62.5 | 54.9 | 69.0 |
| Nov-2020 | 58.0 | 60.5 | 54.0 | 53.2 | 60.2 | 52.9 | 66.4 |
| Dec-2020 | 57.5 | 60.0 | 53.5 | 52.7 | 59.7 | 52.5 | 65.9 |
| Jan-2021 | 54.1 | 54.6 | 47.4 | 41.0 | 49.9 | 58.8 | 61.6 |
| Feb-2021 | 55.4 | 55.9 | 48.5 | 42.0 | 51.0 | 60.2 | 63.0 |
| Mar-2021 | 62.3 | 62.9 | 54.6 | 47.2 | 57.4 | 67.7 | 70.9 |
| Apr-2021 | 63.3 | 63.9 | 55.4 | 48.0 | 58.3 | 68.8 | 72.0 |
| May-2021 | 65.8 | 66.4 | 57.6 | 49.9 | 60.6 | 71.5 | 74.9 |
| Jun-2021 | 69.6 | 70.3 | 61.0 | 52.8 | 64.1 | 75.6 | 79.2 |
| Jul-2021 | 73.1 | 73.8 | 64.0 | 55.4 | 67.4 | 79.4 | 83.2 |
| Aug-2021 | 70.0 | 70.7 | 61.3 | 53.1 | 64.5 | 76.0 | 79.6 |
| Sep-2021 | 67.6 | 68.3 | 59.2 | 51.2 | 62.3 | 73.4 | 76.9 |
| Oct-2021 | 70.6 | 71.3 | 61.8 | 53.5 | 65.1 | 76.7 | 80.3 |
| Nov-2021 | 71.3 | 72.0 | 62.4 | 54.1 | 65.7 | 77.5 | 81.1 |
| Dec-2021 | 72.3 | 73.0 | 63.3 | 54.8 | 66.6 | 78.5 | 82.3 |
| Jan-2022 | 64.5 | 65.1 | 56.5 | 48.9 | 59.4 | 70.1 | 73.4 |

347
348

Table S7: Regional assignment of the passenger load factor for each flight using the origin ICAO airport code. Source: Wikipedia (2022).

| First Letter of ICAO Airport Code | Description | Assigned Region |
|-----------------------------------|---|-----------------|
| A | Western South Pacific | Asia Pacific |
| B | Greenland, Iceland & Kosovo | Europe |
| C | Canada | North America |
| D | Eastern parts of West Africa and Maghreb | Africa |
| E | Northern Europe | Europe |
| F | Central Africa, Southern Africa, and Indian Ocean | Africa |
| G | Western parts of West Africa and Maghreb | Africa |
| H | East Africa and Northeast Africa | Africa |
| K | Contiguous United States | North America |
| L | Southern Europe, Israel, Palestine, and Turkey | Europe |
| M | Central America, Mexico, and Northern/Western Parts of the Caribbean | Latin America |
| N | Most of the South Pacific and New Zealand | Asia Pacific |
| O | Pakistan, Afghanistan, and many West Asian countries | Middle East |
| P | Most of the North Pacific and Kiribati | Asia Pacific |
| R | Western part of the North Pacific | Asia Pacific |
| S | South America | Latin America |
| T | Eastern and southern parts of the Caribbean | Latin America |
| U | Most former Soviet countries | Asia Pacific |
| V | Many South Asian countries, mainland Southeast Asia, Hong Kong, and Macau | Asia Pacific |
| W | Most of Maritime Southeast Asia | Asia Pacific |
| Y | Australia | Asia Pacific |
| Z | China, North Korea, and Mongolia | Asia Pacific |



349
350

Figure S10: Global and regional passenger load factor between 2019 to 2021 assumed in this study.

351 **S4 nvPM emissions**

352 The three methods used in this study to estimate the nvPM number emissions index (EI_n) and
353 mass emissions index (EI_m) are listed in order of priority:

- 354 i. for aircraft-engine types with nvPM measurements available in the ICAO EDB (EASA,
355 2021), the nvPM EI_n and EI_m are estimated using the T_4/T_2 methodology (Teoh et al.,
356 2022a, b),
- 357 ii. for aircraft-engine types where nvPM measurements is not available in the ICAO EDB,
358 the nvPM is estimated according to the methodology of Teoh et al. (2020), where the
359 nvPM EI_m is estimated by using the average value of the Formation and Oxidation
360 (FOX) (Stettler et al., 2013) and Improved FOX (ImFOX) methods (Abrahamson et al.,
361 2016), both of which assumes the emissions profile of single annular combustors, and
362 the nvPM EI_n is estimated from the EI_m using the fractal aggregates (FA) model (Teoh
363 et al., 2019, 2020), and
- 364 iii. for remaining aircraft types where engine-specific data is not available, the nvPM EI_m
365 and EI_n are assumed to be 0.088 g kg^{-1} and 10^{15} kg^{-1} respectively (Stettler et al., 2013;
366 Schumann et al., 2015; Teoh et al., 2020).

367 We describe the T_4/T_2 methodology in detail in Section S4.1 and summarise the FA model in
368 Section S4.2.

369 **S4.1 T_4/T_2 methodology**

370 The T_4/T_2 methodology was originally developed by Teoh et al. (2022a) to estimate the cruise
371 nvPM based on measurements provided by the ICAO EDB. In particular, the nvPM emissions
372 profile for all in-production and new turbofan engines with rated thrust $> 26.7 \text{ kN}$ (~178 unique
373 engines) are constructed using the four ICAO certification test points, and the nvPM emissions
374 at cruise are estimated by linear interpolation relative to the ratio of turbine-inlet (T_4) to

375 compressor-inlet temperature (T_2), a non-dimensional measure of engine thrust settings
376 (Cumpsty and Heyes, 2015).

377 Here, we update the T_4/T_2 methodology with two improvements: (i) an improved estimate of
378 T_4 that is informed using data from the ECLIF II/ND-MAX experimental campaign (Schripp
379 et al., 2022; Bräuer et al., 2021; Voigt et al., 2021), where ground and cruise nvPM EI_n were
380 measured behind an Airbus A320 powered by two IAE V2527-A5 engines; and (ii) an
381 incorporation of the step change in nvPM emission profile for staged combustors such as the
382 double annular combustor (DAC) and the twin annular premixing swirler (TAPS) engine
383 (Boies et al., 2015; Stickles and Barrett, 2013).

384 Fig. S11 summarises the thermodynamic equations used to calculate T_4/T_2 for each waypoint,
385 and the changes applied to improve the T_4/T_2 methodology are highlighted in red. Detailed
386 description of these thermodynamic equations can be found in the Supporting Information
387 §S2.2 of Teoh et al. (2022a). In the original study (Teoh et al., 2022a), the engine thrust settings
388 ($\frac{F}{F_{00,max}}$) was estimated by dividing the fuel mass flow rate at cruise conditions (\dot{m}_f^{Cruise}) by the
389 maximum fuel mass flow rate ($\dot{m}_{f,max}$) that is provided by the ICAO EDB,

$$\frac{F}{F_{00,max}} = \frac{\dot{m}_f^{Cruise}}{\dot{m}_{f,max}}. \quad (S2)$$

390 However, an evaluation of the nvPM EI_n measurements from the ECLIF II/ND-MAX
391 experimental campaign (Schripp et al., 2022; Bräuer et al., 2021; Voigt et al., 2021) suggests
392 that Eq. (S2) could underestimate T_4/T_2 at cruise conditions (Fig. S12a). To address this, we
393 refer to the Fuel Flow Method 2 (FFM2) methodology to convert the \dot{m}_f^{Cruise} to an equivalent
394 fuel mass flow rate at mean sea level conditions (\dot{m}_f^{MSL}) which is then used to estimate $\frac{F}{F_{00,max}}$
395 (DuBois and Paynter, 2006),

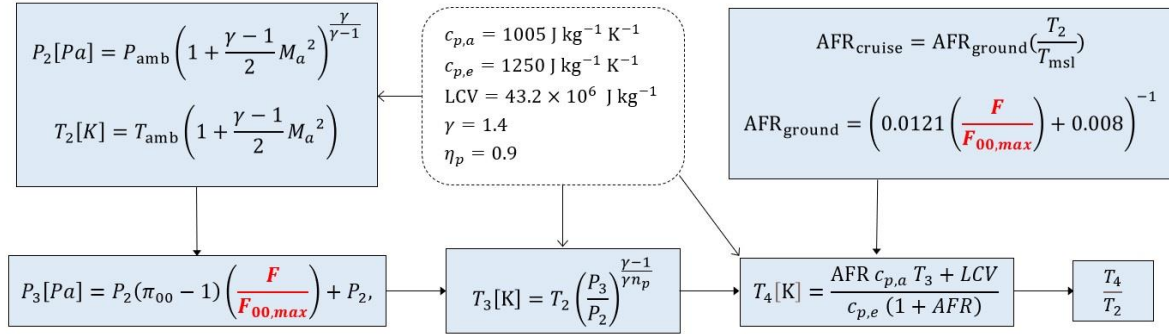
$$\frac{F}{F_{00,\max}} = \frac{\dot{m}_f^{\text{MSL}}}{\dot{m}_{f,\max}} \quad (\text{S3})$$

$$\text{where } \dot{m}_f^{\text{MSL}} = \dot{m}_f^{\text{Cruise}} \left(\frac{T_{\text{amb}}}{T_{\text{MSL}}} \right)^{3.8} \left(\frac{p_{\text{MSL}}}{p_{\text{amb}}} \right) e^{0.2M^2}.$$

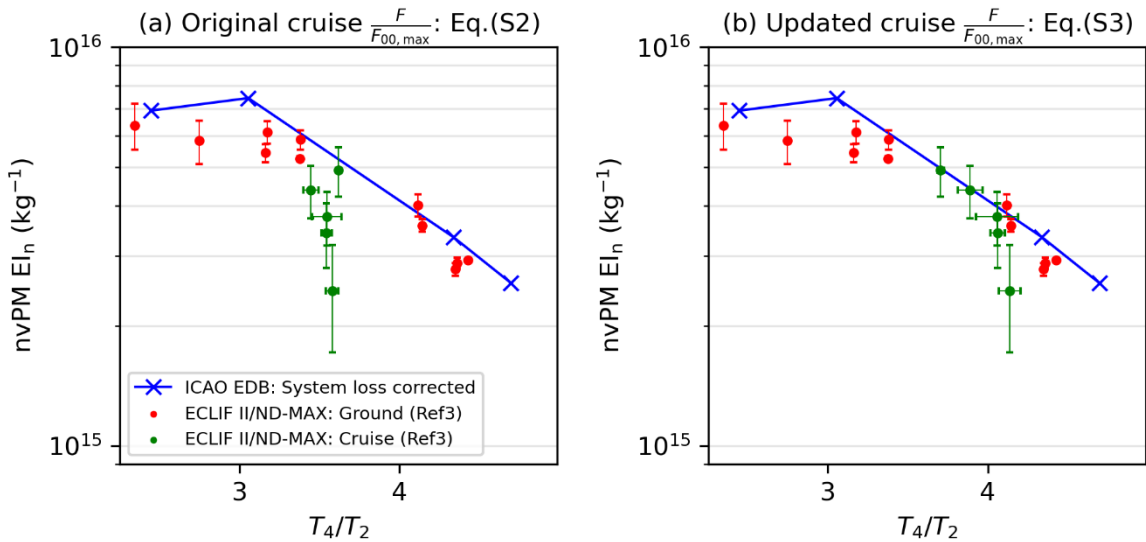
396 Eq. (S3) leads to a 12% increase in T_4/T_2 relative to Eq. (S2), and the cruise nvPM EI_n
 397 measurements are more in-line with the nvPM emissions profile that is provided by the ICAO
 398 EDB (Fig. S12b). Future work is currently ongoing to further assess the performance of the
 399 T_4/T_2 methodology against: (i) cruise nvPM measurements from more recent experimental
 400 campaigns; and (ii) different aircraft-engine combinations.

401 The nvPM emissions profile varies with different engine combustor type (EASA, 2021), and
 402 for most engines, the nvPM EI_n is continuous across the range of $\frac{F}{F_{00,\max}}$. However,
 403 experimental measurements have showed a step change in the nvPM emissions (EI_n and EI_m)
 404 for staged combustors such as the DAC and TAPS engines (Boies et al., 2015; Stickles and
 405 Barrett, 2013): at low $\frac{F}{F_{00,\max}}$ (pilot stage), the engine operates in a fuel-rich environment with
 406 a low air-to-fuel ratio and the nvPM emissions increases with $\frac{F}{F_{00,\max}}$; and at above an $\frac{F}{F_{00,\max}}$
 407 threshold, the engine operates with a higher air-to-fuel ratio (lean combustion stage) and the
 408 nvPM emissions experiences a step change, where the nvPM EI_n and EI_m is lower by up to four
 409 orders of magnitude when compared with the pilot stage. The DAC combustor is primarily
 410 used in the Boeing 777 aircraft (GE90 engine family), while the TAPS combustor (CFM LEAP
 411 and GENx engines) powers the Boeing 737 MAX, a subset of Airbus A320neo and the Boeing
 412 787 Dreamliner (refer to Table S3). To construct the nvPM emissions profile for these staged
 413 combustors, we utilize the four ICAO certification test points (7%, 30%, 85% and 100% $\frac{F}{F_{00,\max}}$)
 414 that is provided by the ICAO EDB (EASA, 2021): a linear interpolation of the nvPM emissions

415 is used when $\frac{F}{F_{00,max}}$ is between 7% and 30%; and above 30% $\frac{F}{F_{00,max}}$, we assume that the engine
 416 operates in the lean combustion mode where the nvPM emissions stays constant with the
 417 average EI_n and EI_m value at 85% and 100% $\frac{F}{F_{00,max}}$.



418
 419 **Figure S11: Thermodynamic equations that is used to calculate the non-dimensional engine thrust settings**
 420 **(T_4/T_2). The engine thrust settings ($\frac{F}{F_{00,max}}$), highlighted in red, is updated in this study and calculated using**
 421 **Eq. (S3) to improve the T_4/T_2 methodology. Detailed descriptions of these equations can be found in the**
 422 **Supporting Information §S2.2 of Teoh et al. (2022a).**



423
 424 **Figure S12: Comparison of the ground (in red) and cruise nvPM EI_n (in green) measured behind an Airbus**
 425 **A320 (powered by two IAE V2527-A5 engines) during the ECLIF II/ND-MAX campaign relative to the**
 426 **four nvPM certification data points provided by the ICAO EDB (in blue), where the non-dimensional**
 427 **engine thrust settings (T_4/T_2) at cruise is calculated using: (a) the original approach outlined in Eq. (S2);**
 428 **and (b) the updated approach outlined in Eq. (S3).**

429 S4.2 Fractal aggregates model

430 The nvPM emissions profile for older aircraft-engine types is not provided by the ICAO EDB
 431 (EASA, 2021) and previous studies used the fractal aggregates (FA) model to estimate the

432 nvPM EI_n for these subset of flights (Teoh et al., 2019, 2020, 2022a, b). The FA model converts
 433 the estimated nvPM EI_m to EI_n with assumptions on the nvPM particle size distribution and
 434 morphology (Teoh et al., 2020, 2019),

$$EI_n = \frac{EI_m}{\rho_0 \left(\frac{\pi}{6}\right) (k_{TEM})^{3-D_{fm}} GMD^\varphi \exp\left(\frac{\varphi^2 \ln(GSD)^2}{2}\right)} \quad (S4)$$

$$\text{where } \varphi = 3D_{TEM} + (1 - D_{TEM})D_{fm}.$$

435 The nvPM EI_m is estimated by taking the average of the outputs provided by the FOX (Stettler
 436 et al., 2013) and ImFOX methods (Abrahamson et al., 2016). GMD is the geometric mean
 437 diameter and is estimated as a function of T_4/T_2 (Teoh et al., 2020),

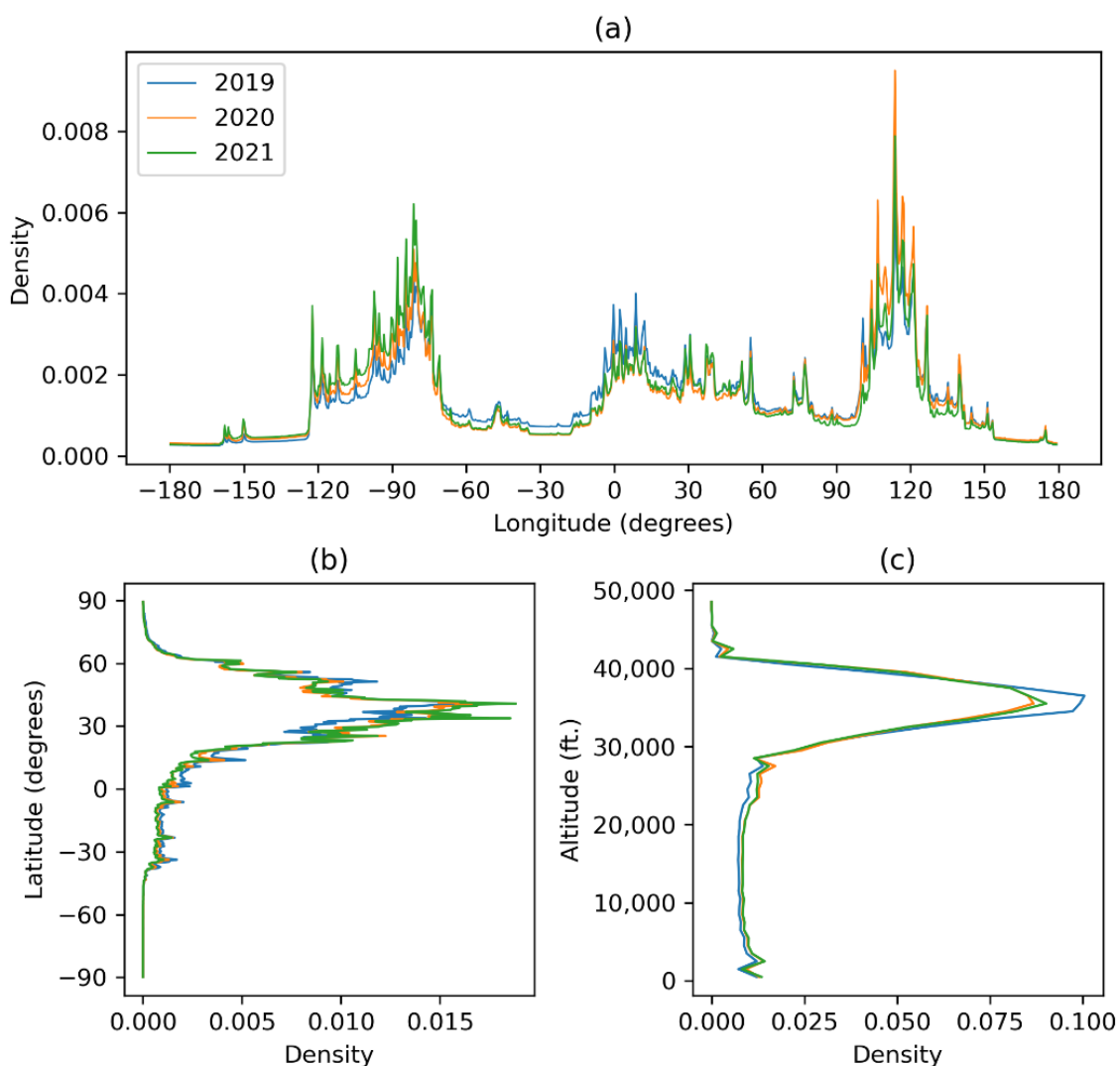
$$GMD[\text{nm}] = 2.5883 \left(\frac{T_4}{T_2}\right)^2 - 5.3723 \left(\frac{T_4}{T_2}\right) + 16.721 + \delta_{\text{loss}}, \quad (S5)$$

438 where δ_{loss} is a correction factor that accounts for particle losses at the instrument sampling
 439 point and is set to a nominal value of -5.75 nm (Teoh et al., 2020). GSD is the geometric
 440 standard deviation (assumed to be 1.80) (Teoh et al., 2020), ρ_0 is the black carbon material
 441 density (1770 kg m^{-3}) (Park et al., 2004), D_{fm} is the mass-mobility exponent of black carbon
 442 aggregates (2.76), and k_{TEM} (1.621×10^{-5}) and D_{TEM} (0.39) are the transmission electron
 443 microscopy prefactor and exponent coefficients respectively (Dastanpour and Rogak, 2014).

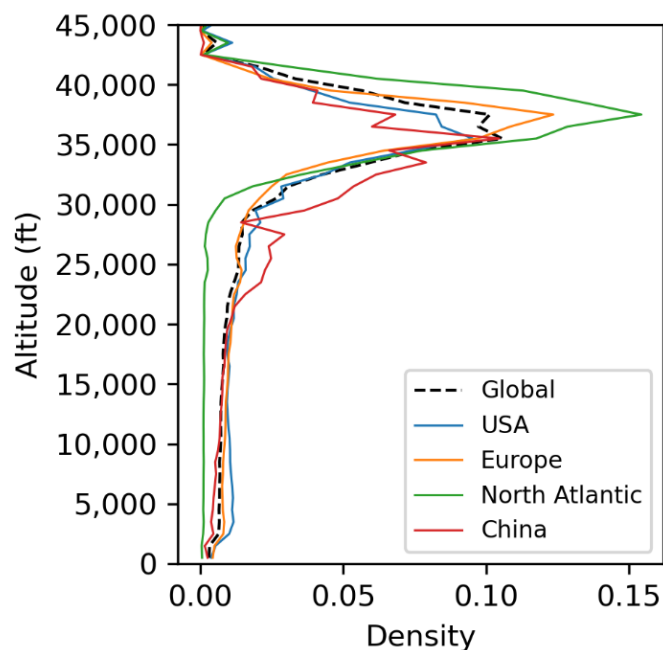
444 **S5 Global aviation emissions inventory**

445 The global aviation emissions inventory for 2019–2021 is named as the Global Aviation
 446 Emissions Inventory based on ADS-B (GAIA). Fig. S13 shows the distribution of the 2019–
 447 2021 annual fuel consumption by longitude, latitude, and altitude, where ~92% of the 2019
 448 annual fuel consumption occurred in the Northern Hemisphere. Fig. 3b in the main text shows
 449 that the mean nvPM EI_m and EI_n above 45,000 feet (0.39 g kg^{-1} and $4.5 \times 10^{15} \text{ kg}^{-1}$) are around
 450 4–5 times larger than the global mean values (0.076 g kg^{-1} and $1.0 \times 10^{15} \text{ kg}^{-1}$) because of a

451 higher prevalence of private business jets whose mean nvPM EI_m and EI_n can be up to 0.58 g
 452 kg^{-1} and $7 \times 10^{15} kg^{-1}$ respectively (Table S8). Tables S9 and S10 break down the 2020 and
 453 2021 global aviation activity, fuel consumption, and emissions into 11 key regions. In 2019,
 454 the mean fuel consumption per flight distance in China ($4.99 kg km^{-1}$) is 52% and 21% larger
 455 than the US ($3.29 kg km^{-1}$) and Europe ($4.14 kg km^{-1}$) respectively (Table 4 in the main text),
 456 and this could be due to the: (i) higher proportion of flights cruising at lower altitudes of
 457 between 25,000 and 35,000 feet (44% of the total flight distance flown) when compared to
 458 other regions (31% of the flight distance flown globally) (Fig. S14); and (ii) differences in the
 459 fleet composition mix (proportion of narrow-body-to-wide-body aircraft) in different regions.



460
 461 **Figure S13: Probability density function of the annual fuel consumption from GAIA by: (a) longitude; (b)**
 462 **latitude; and (c) altitude for 2019 (in blue), 2020 (in orange) and 2021 (in green).**



463
 464 **Figure S14: Probability density function of the 2019 annual flight distance flown in GAIA by altitude across**
 465 **the globe (black dotted line), and over the USA (in blue), Europe (in orange), North Atlantic (in green) and**
 466 **China (in red).**

467 **Table S8: Top 10 commonly used aircraft types above 45,000 feet and their mean nvPM EI_n in GAIA.**

| Aircraft type | % of distance flown above 45,000 feet | Mean nvPM EI _n ($\times 10^{15} \text{ kg}^{-1}$) | Mean nvPM EI _m (g kg^{-1}) |
|---------------|---------------------------------------|--|--|
| GLF5 | 26.4% | 7.14 | 0.52 |
| GLF6 | 17.2% | 6.81 | 0.55 |
| C750 | 16.5% | 0.32 | 0.036 |
| GLEX | 14.7% | 7.12 | 0.055 |
| GL5T | 4.2% | 7.09 | 0.54 |
| F2TH | 3.7% | 4.51 | 0.59 |
| FA7X | 3.4% | 2.29 | 0.084 |
| LJ45 | 2.2% | 0.26 | 0.025 |
| LJ75 | 1.2% | 0.31 | 0.029 |
| F900 | 1.1% | 0.28 | 0.028 |

468 GAIA, which contains 103.7 million unique flight trajectories between 2019 and 2021, is used
 469 to provide statistics on the distribution of air traffic activity and emissions by flight mission
 470 profile. Tables S11 and S12 categorises the 2020–2021 global air traffic activity and emissions
 471 into three groups based on their flight duration.

Table S9: Regional aviation activity, fuel consumption and emissions for 2020.

| Regional statistics: 2020 | Global | USA | Europe | East Asia | SEA | Latin America | Africa & Middle East | China | India | North Atlantic | North Pacific | Arctic Region |
|---|--------|-------|--------|-----------|-------|---------------|----------------------|-------|-------|----------------|---------------|---------------|
| Distance travelled (x10 ⁹ km) | 34.49 | 11.27 | 3.592 | 6.298 | 1.569 | 1.072 | 2.015 | 6.848 | 1.257 | 1.159 | 1.610 | 0.160 |
| - Percentage by region* | - | 33% | 10% | 18% | 4.5% | 3.1% | 5.8% | 20% | 3.6% | 3.4% | 4.7% | 0.5% |
| Air traffic density (km ⁻¹ h ⁻¹) | 0.008 | 0.080 | 0.062 | 0.044 | 0.012 | 0.003 | 0.004 | 0.036 | 0.016 | 0.012 | 0.008 | 0.001 |
| Fuel burn (Tg) | 146 | 32.4 | 14.6 | 29.5 | 7.73 | 4.45 | 9.91 | 31.6 | 6.20 | 6.83 | 10.8 | 1.14 |
| - Percentage by region* | - | 22% | 10% | 20% | 5.3% | 3.0% | 6.8% | 22% | 4.2% | 4.7% | 7.4% | 0.8% |
| Fuel burn per dist. (kg km ⁻¹) | 4.242 | 2.875 | 4.065 | 4.684 | 4.927 | 4.151 | 4.918 | 4.614 | 4.932 | 5.893 | 6.714 | 7.125 |
| CO ₂ (Tg) | 462 | 102 | 46.1 | 93.2 | 24.4 | 14.1 | 31.3 | 100 | 19.6 | 21.6 | 34.1 | 3.60 |
| H ₂ O (Tg) | 180 | 39.9 | 18.0 | 36.3 | 9.51 | 5.47 | 12.2 | 38.9 | 7.63 | 8.40 | 13.3 | 1.40 |
| OC (Gg) | 2.93 | 0.648 | 0.292 | 0.590 | 0.155 | 0.089 | 0.198 | 0.632 | 0.124 | 0.137 | 0.216 | 0.023 |
| SO ₂ (Gg) | 176 | 38.9 | 17.5 | 35.4 | 9.28 | 5.34 | 11.9 | 37.9 | 7.44 | 8.20 | 13.0 | 1.37 |
| S ^{VI} (Gg) | 3.58 | 0.793 | 0.358 | 0.722 | 0.189 | 0.109 | 0.243 | 0.774 | 0.152 | 0.167 | 0.265 | 0.028 |
| NO _x (Tg) | 2.26 | 0.441 | 0.222 | 0.456 | 0.130 | 0.070 | 0.160 | 0.483 | 0.103 | 0.108 | 0.183 | 0.020 |
| - Percentage by region* | - | 20% | 10% | 20% | 5.8% | 3.1% | 7.1% | 21% | 4.6% | 4.8% | 8.1% | 0.9% |
| CO (Gg) | 227 | 72.0 | 30.2 | 46.3 | 12.5 | 6.82 | 13.0 | 47.5 | 7.73 | 4.07 | 10.1 | 0.561 |
| - Percentage by region* | - | 32% | 13% | 20% | 5.5% | 3.0% | 5.7% | 21% | 3.4% | 1.8% | 4.4% | 0.2% |
| HC (Gg) | 20.9 | 7.55 | 2.50 | 3.46 | 0.95 | 0.53 | 1.21 | 3.52 | 0.59 | 0.51 | 1.03 | 0.066 |
| - Percentage by region* | - | 36% | 12% | 17% | 4.5% | 2.5% | 5.8% | 17% | 2.8% | 2.4% | 4.9% | 0.3% |
| nvPM mass (Gg) | 9.93 | 2.86 | 1.06 | 2.13 | 0.540 | 0.310 | 0.600 | 2.25 | 0.363 | 0.325 | 0.452 | 0.036 |
| - Percentage by region* | - | 29% | 11% | 21% | 5.4% | 3.1% | 6.0% | 23% | 3.7% | 3.3% | 4.6% | 0.4% |
| nvPM number (x10 ²⁶) | 1.464 | 0.430 | 0.158 | 0.335 | 0.071 | 0.042 | 0.080 | 0.363 | 0.063 | 0.039 | 0.070 | 0.005 |
| - Percentage by region* | - | 29% | 11% | 23% | 4.8% | 2.9% | 5.5% | 25% | 4.3% | 2.7% | 4.8% | 0.3% |
| Mean EI NO _x (g kg ⁻¹) | 15.4 | 13.6 | 15.2 | 15.5 | 16.8 | 15.7 | 16.1 | 15.3 | 16.6 | 15.8 | 16.9 | 17.4 |
| Mean EI CO (g kg ⁻¹) | 1.55 | 2.22 | 2.07 | 1.57 | 1.62 | 1.53 | 1.31 | 1.50 | 1.25 | 0.60 | 0.93 | 0.49 |
| Mean EI HC (g kg ⁻¹) | 0.143 | 0.233 | 0.171 | 0.117 | 0.123 | 0.119 | 0.122 | 0.112 | 0.095 | 0.074 | 0.096 | 0.058 |
| Mean nvPM EI _m (g kg ⁻¹) | 0.068 | 0.088 | 0.073 | 0.072 | 0.070 | 0.070 | 0.061 | 0.071 | 0.059 | 0.048 | 0.042 | 0.032 |
| Mean nvPM EI _n (x10 ¹⁵ kg ⁻¹) | 1.001 | 1.328 | 1.085 | 1.136 | 0.913 | 0.954 | 0.810 | 1.149 | 1.010 | 0.569 | 0.646 | 0.413 |

*: The percentages of each region do not add up to 100% because there are some overlapping between the regional bounding boxes; and when taken together, these regions do not cover 100% of Earth's surface area (refer to Fig. 1 and Table 2 in the main text).

Table S10: Regional aviation activity, fuel consumption and emissions for 2021.

| Regional statistics: 2021 | Global | USA | Europe | East Asia | SEA | Latin America | Africa & Middle East | China | India | North Atlantic | North Pacific | Arctic Region |
|---|--------|-------|--------|-----------|-------|---------------|----------------------|-------|-------|----------------|---------------|---------------|
| Distance travelled (x10 ⁹ km) | 41.91 | 15.17 | 4.475 | 5.948 | 1.208 | 1.479 | 2.795 | 6.654 | 1.438 | 1.441 | 1.736 | 0.193 |
| - Percentage by region* | - | 36% | 11% | 14% | 2.9% | 3.5% | 6.7% | 16% | 3.4% | 3.4% | 4.1% | 0.5% |
| Air traffic density (km ⁻¹ h ⁻¹) | 0.009 | 0.108 | 0.077 | 0.042 | 0.009 | 0.004 | 0.005 | 0.035 | 0.018 | 0.014 | 0.008 | 0.001 |
| Fuel burn (Tg) | 166 | 42.5 | 16.8 | 27.8 | 6.14 | 5.64 | 12.59 | 30.2 | 6.39 | 8.35 | 11.5 | 1.33 |
| - Percentage by region* | - | 26% | 10% | 17% | 3.7% | 3.4% | 7.6% | 18% | 3.9% | 5.0% | 6.9% | 0.8% |
| Fuel burn per dist. (kg km ⁻¹) | 3.956 | 2.802 | 3.761 | 4.670 | 5.084 | 3.811 | 4.504 | 4.540 | 4.440 | 5.795 | 6.607 | 6.909 |
| CO ₂ (Tg) | 524 | 134 | 53.2 | 87.8 | 19.4 | 17.8 | 39.8 | 95.4 | 20.2 | 26.4 | 36.2 | 4.21 |
| H ₂ O (Tg) | 204 | 52.3 | 20.7 | 34.2 | 7.55 | 6.93 | 15.5 | 37.2 | 7.85 | 10.27 | 14.1 | 1.64 |
| OC (Gg) | 3.32 | 0.850 | 0.337 | 0.556 | 0.123 | 0.113 | 0.252 | 0.604 | 0.128 | 0.167 | 0.229 | 0.027 |
| SO ₂ (Gg) | 199 | 51.0 | 20.2 | 33.3 | 7.37 | 6.76 | 15.1 | 36.3 | 7.66 | 10.02 | 13.8 | 1.60 |
| S ^{VI} (Gg) | 4.06 | 1.04 | 0.412 | 0.680 | 0.150 | 0.138 | 0.308 | 0.740 | 0.156 | 0.204 | 0.281 | 0.033 |
| NO _x (Tg) | 2.55 | 0.589 | 0.253 | 0.433 | 0.105 | 0.087 | 0.202 | 0.463 | 0.104 | 0.136 | 0.195 | 0.024 |
| - Percentage by region* | - | 23% | 10% | 17% | 4.1% | 3.4% | 7.9% | 18% | 4.1% | 5.3% | 7.7% | 0.9% |
| CO (Gg) | 272 | 93.2 | 36.4 | 47.4 | 10.2 | 9.56 | 18.3 | 49.6 | 8.99 | 5.07 | 11.2 | 0.703 |
| - Percentage by region* | - | 34% | 13% | 17% | 3.8% | 3.5% | 6.7% | 18% | 3.3% | 1.9% | 4.1% | 0.3% |
| HC (Gg) | 25.0 | 9.88 | 2.99 | 3.47 | 0.82 | 0.72 | 1.60 | 3.59 | 0.63 | 0.58 | 1.15 | 0.081 |
| - Percentage by region* | - | 40% | 12% | 14% | 3.3% | 2.9% | 6.4% | 14% | 2.5% | 2.3% | 4.6% | 0.3% |
| nvPM mass (Gg) | 11.0 | 3.73 | 1.15 | 1.84 | 0.369 | 0.382 | 0.731 | 1.99 | 0.321 | 0.389 | 0.430 | 0.038 |
| - Percentage by region* | - | 34% | 10% | 17% | 3.4% | 3.5% | 6.7% | 18% | 2.9% | 3.5% | 3.9% | 0.3% |
| nvPM number (x10 ²⁶) | 1.663 | 0.560 | 0.179 | 0.302 | 0.048 | 0.054 | 0.103 | 0.337 | 0.065 | 0.045 | 0.069 | 0.005 |
| - Percentage by region* | - | 34% | 11% | 18% | 2.9% | 3.2% | 6.2% | 20% | 3.9% | 2.7% | 4.2% | 0.3% |
| Mean EI NO _x (g kg ⁻¹) | 15.4 | 13.9 | 15.0 | 15.6 | 17.2 | 15.5 | 16.0 | 15.3 | 16.3 | 16.3 | 17.0 | 18.0 |
| Mean EI CO (g kg ⁻¹) | 1.64 | 2.19 | 2.16 | 1.71 | 1.66 | 1.70 | 1.45 | 1.64 | 1.41 | 0.61 | 0.98 | 0.53 |
| Mean EI HC (g kg ⁻¹) | 0.151 | 0.232 | 0.178 | 0.125 | 0.133 | 0.127 | 0.127 | 0.119 | 0.099 | 0.070 | 0.100 | 0.060 |
| Mean nvPM EI _m (g kg ⁻¹) | 0.066 | 0.088 | 0.068 | 0.066 | 0.060 | 0.068 | 0.058 | 0.066 | 0.050 | 0.047 | 0.037 | 0.029 |
| Mean nvPM EI _n (x10 ¹⁵ kg ⁻¹) | 1.003 | 1.317 | 1.061 | 1.088 | 0.774 | 0.950 | 0.817 | 1.116 | 1.024 | 0.540 | 0.604 | 0.381 |

*: The percentages of each region do not add up to 100% because there are some overlapping between the regional bounding boxes; and when taken together, these regions do not cover 100% of Earth's surface area (refer to Fig. 1 and Table 2 in the main text).

479

Table S11: Breakdown of aviation activity, fuel consumption and emissions for 2020 by flight duration.

| Flight-level statistics: 2020 | All flights | Short-haul ($t \leq 3\text{h}$) | | Medium-haul ($3 < t \leq 6$) | | Long-haul ($t > 6$) | |
|---|-------------|-----------------------------------|---------|--------------------------------|---------|-----------------------|---------|
| | | Value | % total | Value | % total | Value | % total |
| Number of flights | 27,911,214 | 24,415,965 | 87.5% | 2,563,329 | 9.2% | 931,920 | 3.3% |
| Number of night flights ^a | 4,375,917 | 3,707,150 | 84.7% | 507,657 | 11.6% | 161,110 | 3.7% |
| Distance travelled ($\times 10^9$ km) | 34.50 | 19.47 | 56.4% | 7.737 | 22.4% | 7.292 | 21.1% |
| Fuel burn (Tg) | 146 | 60.4 | 41.3% | 31.2 | 21.3% | 54.7 | 37.4% |
| Fuel burn per dist. (kg km^{-1}) | 4.241 | 3.102 | - | 4.035 | - | 7.499 | - |
| Mean flight time (h) | 1.76 | 1.27 | - | 3.95 | - | 9.08 | - |
| Mean flight length (km) | 1236 | 797 | - | 3018 | - | 7825 | - |
| Mean aircraft mass (kg) | 49593 | 39896 | - | 86607 | - | 211559 | - |
| - Fuel fraction ^b | 7.20% | 5.69% | - | 15.2% | - | 26.0% | - |
| CO ₂ (Tg) | 462 | 191 | 41.3% | 99 | 21.3% | 173 | 37.4% |
| NO _x (Tg) | 2.26 | 0.829 | 36.7% | 0.447 | 19.8% | 0.983 | 43.5% |
| CO (Gg) | 227 | 147 | 64.8% | 40.4 | 17.8% | 39.4 | 17.4% |
| HC (Gg) | 20.9 | 12.3 | 58.9% | 4.19 | 20.0% | 4.40 | 21.1% |
| nvPM mass (Gg) | 9.93 | 5.35 | 53.9% | 2.38 | 24.0% | 2.20 | 22.2% |
| nvPM number ($\times 10^{26}$) | 1.46 | 0.864 | 59.2% | 0.353 | 24.2% | 0.247 | 16.9% |
| Mean EI NO _x (g kg^{-1}) | 15.45 | 13.73 | - | 14.32 | - | 17.98 | - |
| Mean EI CO (g kg^{-1}) | 1.55 | 2.43 | - | 1.29 | - | 0.72 | - |
| Mean EI HC (g kg^{-1}) | 0.14 | 0.20 | - | 0.13 | - | 0.08 | - |
| Mean nvPM EI _m (g kg^{-1}) | 0.068 | 0.089 | - | 0.076 | - | 0.040 | - |
| Mean nvPM EI _n ($\times 10^{15} \text{kg}^{-1}$) | 0.998 | 1.430 | - | 1.131 | - | 0.452 | - |

480

^a: Night flights are identified when their mean solar direct radiation (SDR) throughout their flight trajectory is $< 1 \text{ W m}^{-2}$.

481

^b: Fuel fraction = total fuel mass/initial aircraft mass

482

Table S12: Breakdown of aviation activity, fuel consumption and emissions for 2021 by flight duration.

| Flight-level statistics: 2021 | All flights | Short-haul ($t \leq 3\text{h}$) | | Medium-haul ($3 < t \leq 6$) | | Long-haul ($t > 6$) | |
|---|-------------|-----------------------------------|---------|--------------------------------|---------|-----------------------|---------|
| | | Value | % total | Value | % total | Value | % total |
| Number of flights | 35,576,376 | 31,277,810 | 87.9% | 3,278,356 | 9.2% | 1,020,210 | 2.9% |
| Number of night flights ^a | 4,847,915 | 4,120,217 | 85.0% | 568,596 | 11.7% | 159,102 | 3.3% |
| Distance travelled ($\times 10^9$ km) | 41.90 | 24.06 | 57.4% | 9.853 | 23.5% | 7.994 | 19.1% |
| Fuel burn (Tg) | 166 | 70.2 | 42.4% | 37.8 | 22.8% | 57.8 | 34.8% |
| Fuel burn per dist. (kg km^{-1}) | 3.957 | 2.919 | - | 3.837 | - | 7.227 | - |
| Mean flight time (h) | 1.74 | 1.26 | - | 3.95 | - | 9.06 | - |
| Mean flight length (km) | 1178 | 769 | - | 3005 | - | 7836 | - |
| Mean aircraft mass (kg) | 46533 | 37440 | - | 82687 | - | 207952 | - |
| - Fuel fraction ^b | 6.98% | 5.53% | - | 14.9% | - | 25.6% | - |
| CO ₂ (Tg) | 524 | 222 | 42.4% | 119 | 22.8% | 182 | 34.8% |
| NO _x (Tg) | 2.55 | 0.97 | 37.8% | 0.542 | 21.3% | 1.04 | 40.8% |
| CO (Gg) | 272 | 179 | 65.8% | 49.9 | 18.3% | 42.7 | 15.7% |
| HC (Gg) | 25.0 | 15.2 | 60.8% | 5.26 | 21.0% | 4.56 | 18.2% |
| nvPM mass (Gg) | 11.0 | 5.98 | 54.5% | 2.79 | 25.4% | 2.21 | 20.1% |
| nvPM number ($\times 10^{26}$) | 1.66 | 0.984 | 59.3% | 0.427 | 25.7% | 0.252 | 15.2% |
| Mean EI NO _x (g kg^{-1}) | 15.38 | 13.74 | - | 14.33 | - | 18.00 | - |
| Mean EI CO (g kg^{-1}) | 1.64 | 2.55 | - | 1.32 | - | 0.74 | - |
| Mean EI HC (g kg^{-1}) | 0.15 | 0.22 | - | 0.14 | - | 0.08 | - |
| Mean nvPM EI _m (g kg^{-1}) | 0.066 | 0.085 | - | 0.074 | - | 0.038 | - |
| Mean nvPM EI _n ($\times 10^{15} \text{kg}^{-1}$) | 1.001 | 1.401 | - | 1.129 | - | 0.436 | - |

483

^a: Night flights are identified when their mean solar direct radiation (SDR) throughout their flight trajectory is $< 1 \text{ W m}^{-2}$.

484

^b: Fuel fraction = total fuel mass/initial aircraft mass

485 **S6 Comparison with other studies**

486 Table S13 compares the 2019–2020 annual fuel consumption, emissions, and mean EI’s from
 487 GAIA relative to those derived from Quadros et al. (2022). The 2019 annual fuel consumption
 488 from GAIA (283 Tg) is 4.7% lower than Quadros et al. (2022) (297 Tg). Fig. S15 compares
 489 the spatial distribution of the 2019 annual fuel consumption between our study and Quadros et
 490 al. (2022): the fuel consumption from Quadros et al. (2022) are more concentrated along
 491 established flight corridors because monthly-averaged flight trajectories were used; while
 492 GAIA uses the actual flight trajectories flown which causes the fuel consumption to be more
 493 spatially dispersed.

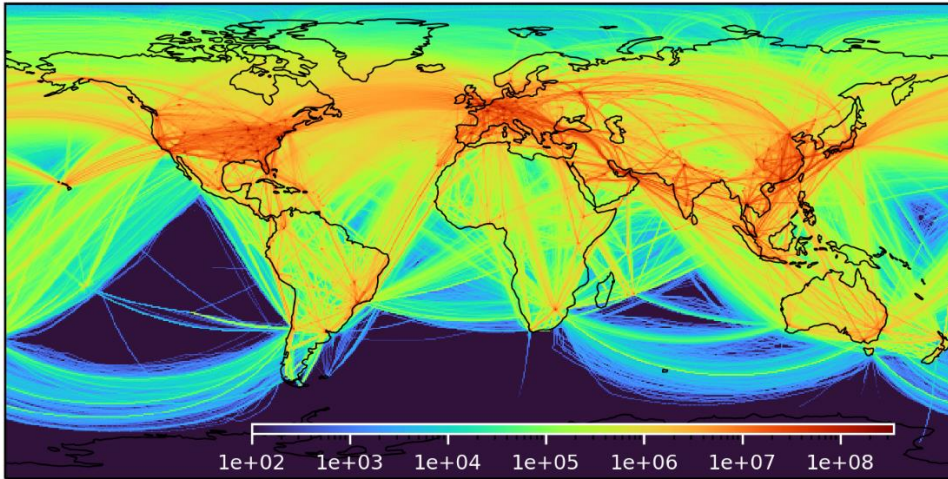
494 **Table S13: Comparison of the 2019–2020 annual fuel consumption, emissions and mean EI’s derived**
 495 **from GAIA versus those from Quadros et al. (2022) using Flightradar24 data.**

| Annual statistics | GAIA | | Quadros et al. (2022) | | % difference | |
|---|-------|-------|-----------------------|-------|--------------|-------|
| | 2019 | 2020 | 2019 | 2020 | 2019 | 2020 |
| Fuel burn (Tg) | 283 | 146 | 297 | 157 | -4.7% | -6.9% |
| CO ₂ (Tg) | 893 | 462 | 937 | 496 | -4.7% | -6.9% |
| H ₂ O (Tg) | 348 | 180 | 367 | 194 | -5.2% | -7.0% |
| NO _x (Tg) | 4.49 | 2.26 | 4.62 | 2.44 | -2.8% | -7.4% |
| CO (Gg) | 400 | 227 | 814 | 569 | -51% | -60% |
| HC (Gg) | 33.9 | 20.9 | 42.6 | 27.3 | -20% | -23% |
| nvPM mass (Gg) | 21.4 | 9.93 | 9.68 | 4.79 | 121% | 107% |
| nvPM number (x10 ²⁶) | 2.83 | 1.46 | 3.47 | 1.73 | -18% | -16% |
| Mean EI NO _x (g kg ⁻¹) | 15.9 | 15.4 | 15.6 | 15.5 | 2.2% | -0.6% |
| Mean EI CO (g kg ⁻¹) | 1.42 | 1.55 | 2.74 | 3.62 | -48% | -57% |
| Mean EI HC (g kg ⁻¹) | 0.120 | 0.143 | 0.143 | 0.174 | -16% | -18% |
| Mean nvPM EI _m (g kg ⁻¹) | 0.076 | 0.068 | 0.033 | 0.031 | 132% | 122% |
| Mean nvPM EI _n (x10 ¹⁵ kg ⁻¹) | 1.00 | 1.00 | 1.17 | 1.10 | -14.3% | -9.4% |

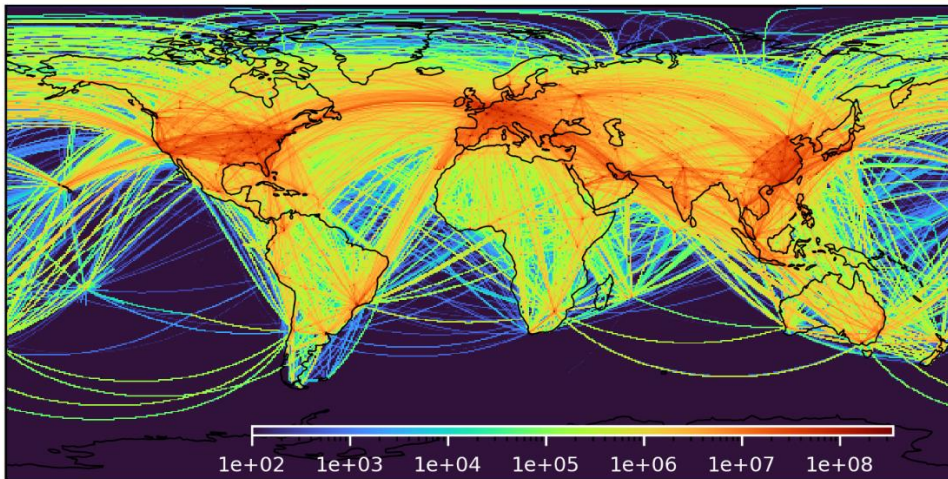
496 Differences in the 2019 mean EI’s from different pollutants are between -48% and +132%. In
 497 particular, GAIA estimates a lower EI CO (1.4 g kg⁻¹) and HC (0.12 g kg⁻¹) when compared to
 498 Quadros et al. (2022) (2.7 g kg⁻¹ for CO and 0.14 g kg⁻¹ for HC), and these discrepancies could
 499 be caused by the exclusion of ground emissions in GAIA where the EI’s of these pollutants are
 500 generally at a maximum during the taxi phase (Fig. S18 and S19). Fig. S16 breaks down the
 501 fuel consumption and mean EI’s from the two studies by altitude. At cruise altitudes (between
 502 30,000 and 40,000 feet), large differences are observed in the total fuel consumption because

503 Quadros et al. (2022) assumed a constant cruise altitude for each aircraft type in the modelled
504 flight trajectory. There are also large discrepancies in the EI's of CO, HC and nvPM EI_m
505 specifically at altitudes below 10,000 feet and above 30,000 feet, and these likely arise from
506 the treatment of aircraft-engine assignments between both studies. Aircraft-engine assignments
507 in GAIA uses a global fleet database (Cirium, 2022) whenever possible to obtain the specific
508 aircraft variant and engine model (covering 59% of all flights or 79% of flights by jet aircraft,
509 SI §S2), while Quadros et al. (2022) compiled data on the aircraft-type-specific engine market
510 share and aggregated the global emissions with a weighted average of their respective market
511 share. Fig. S17 to S21 illustrates the variations in the emissions profile of NO_x, CO, HC, and
512 nvPM for different aircraft-engine combinations, where specific aircraft types such as the
513 Airbus A320, A20N, and Boeing 787 have large variations among the different engine options
514 available. Fig. S16f also shows that the difference in nvPM EI_m from both studies generally
515 increases with altitude, and this could be due to use of the Döpelheuer & Lecht relation (Peck
516 et al., 2013; Döpelheuer and Lecht, 1998) in Quadros et al. (2022) to scale nvPM emissions
517 from ground to cruise which could underestimate the nvPM EI_m (Abrahamson et al., 2016).

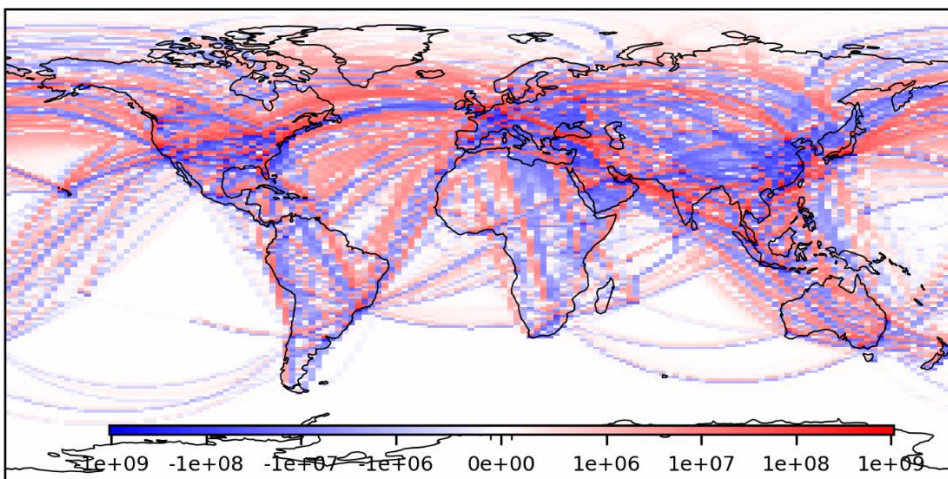
(a) 2019 fuel consumption (kg): GAIA



(b) 2019 fuel consumption (kg): Quadros et al. (2022)

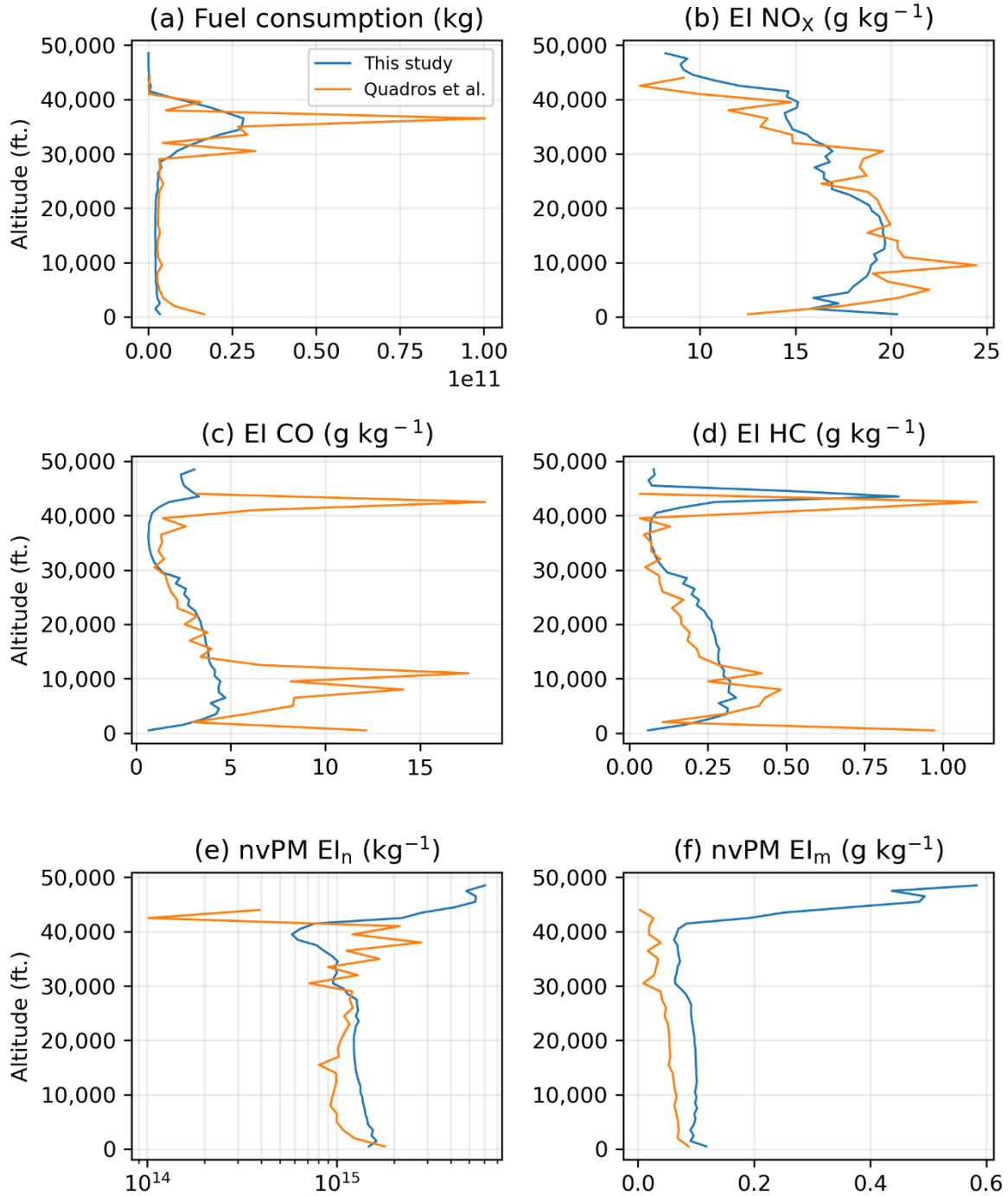


(c) Difference in 2019 fuel burn (kg): GAIA - Quadros et al. (2022)



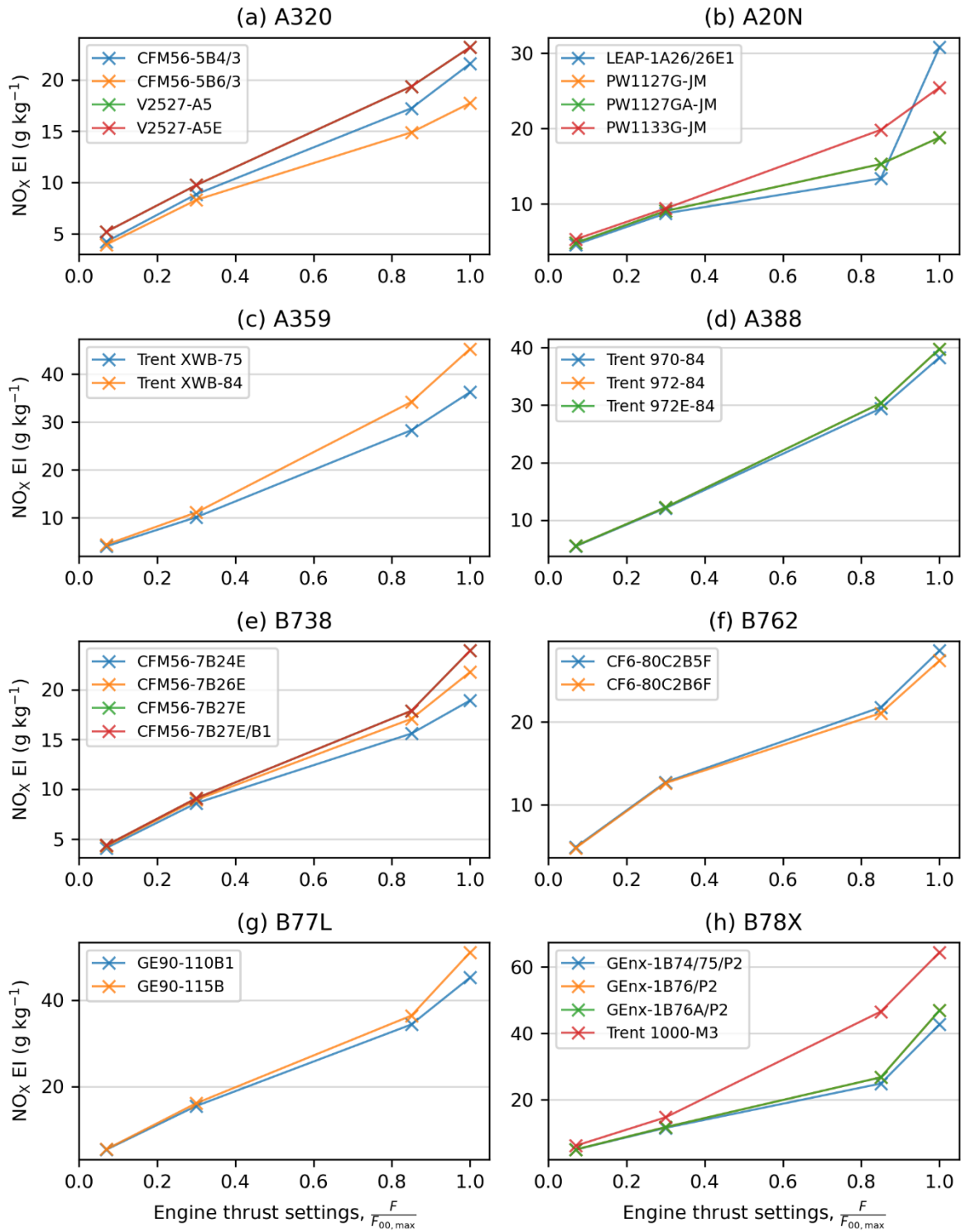
518

519 **Figure S15: Spatial distribution of the 2019 annual fuel consumption from (a) GAIA with actual flight**
520 **trajectories versus (b) estimates from Quadros et al. (2022) which used monthly-averaged flight**
521 **trajectories, and (c) the absolute difference in annual fuel consumption between (a) and (b). Basemap**
522 **plotted using Cartopy 0.21.1 © Natural Earth; license: public domain.**



523

524 **Figure S16: Breakdown of the 2019 annual: (a) fuel consumption, the EI's of (b) NO_x, (c) CO, (d) HC, and**
 525 **the nvPM (e) EI_n and (f) EI_m that is derived from this study (blue lines) versus those from Quadros et al.**
 526 **(2022) (orange lines).**

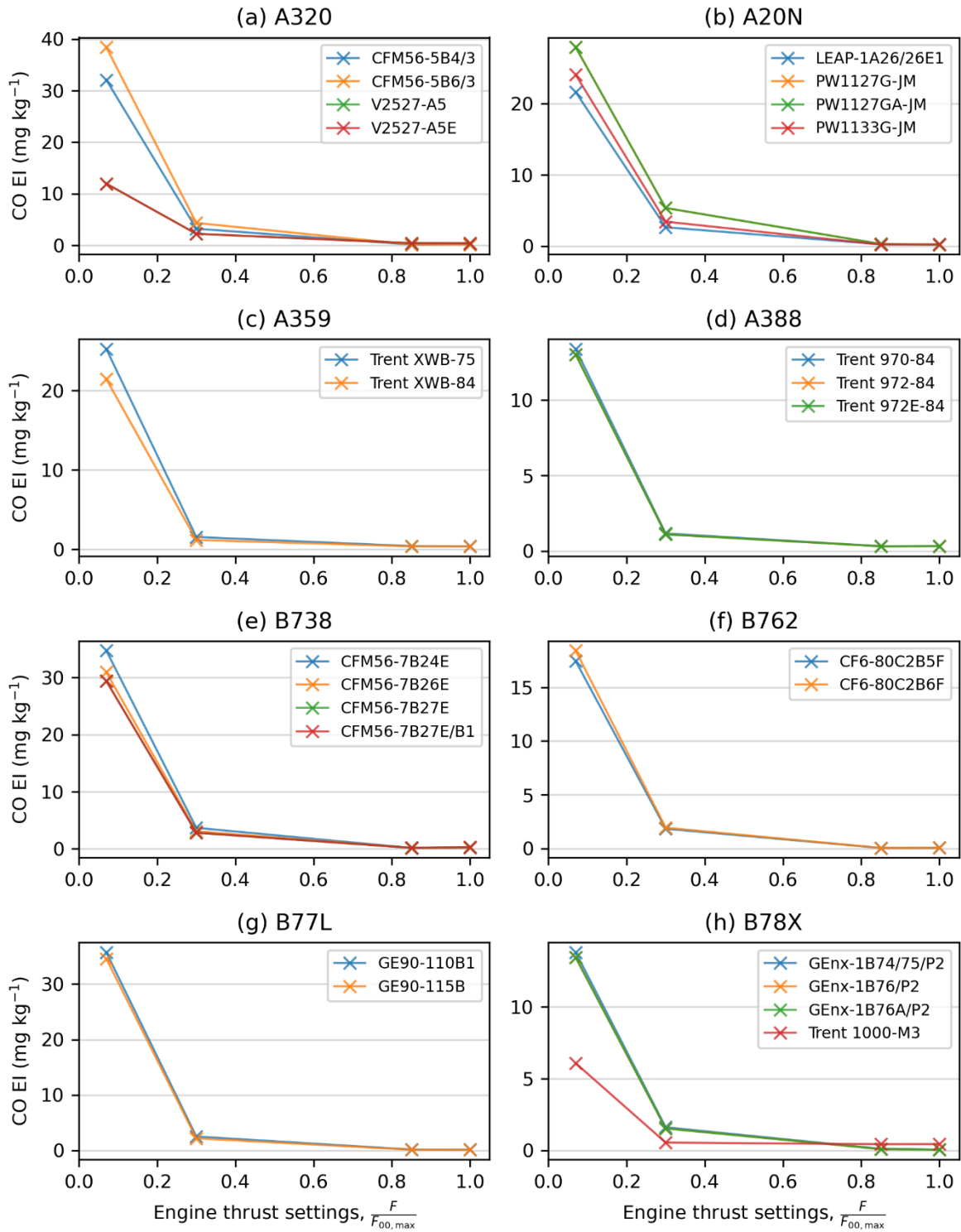


527

528

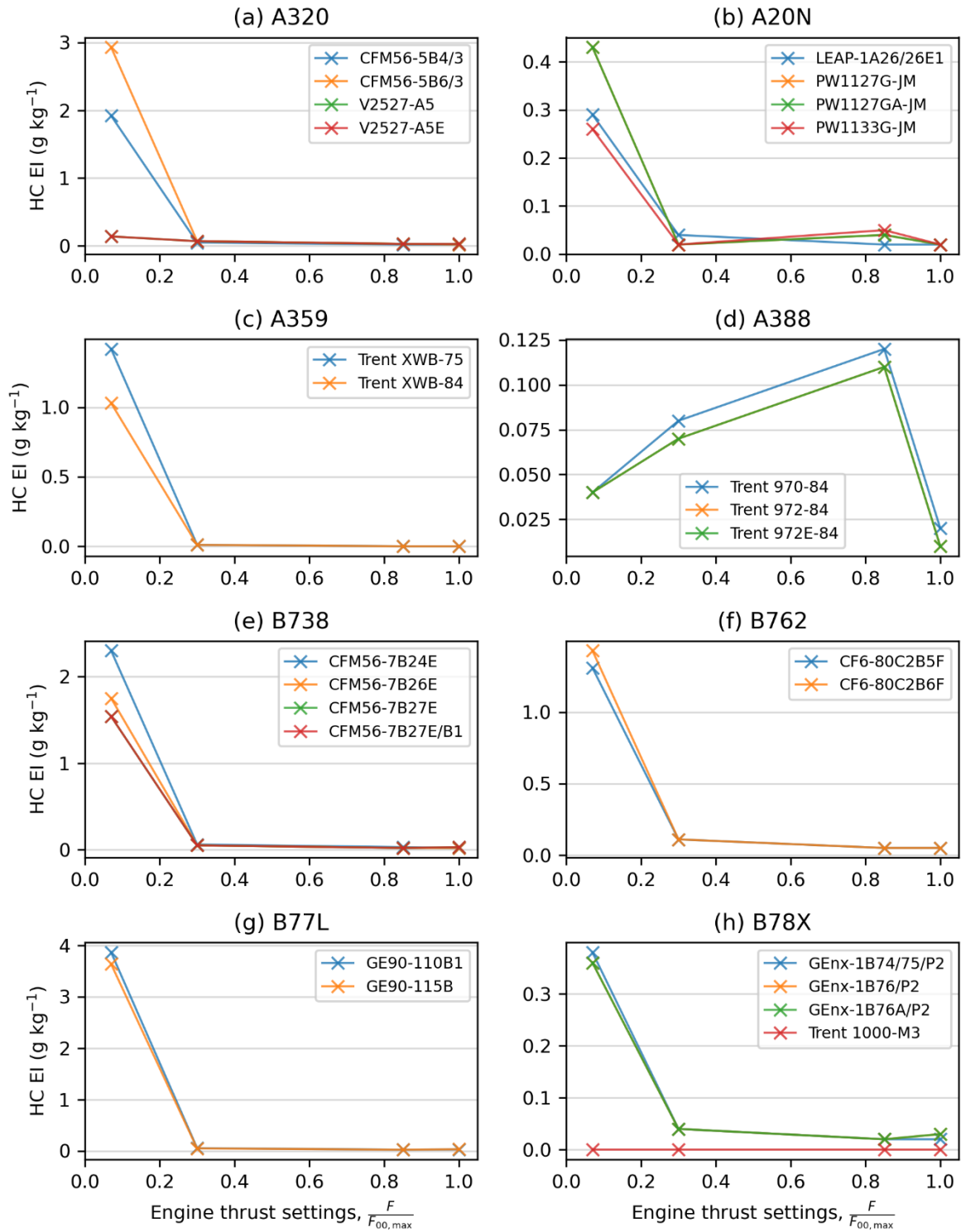
529

Figure S17: ICAO EDB measurements of the NO_x EI at the four certification test points (7%, 30%, 85% and 100% engine thrust settings) for selected aircraft-engine pairs.



530
531
532

Figure S18: ICAO EDB measurements of the CO EI at the four certification test points (7%, 30%, 85% and 100% engine thrust settings) for selected aircraft-engine pairs.

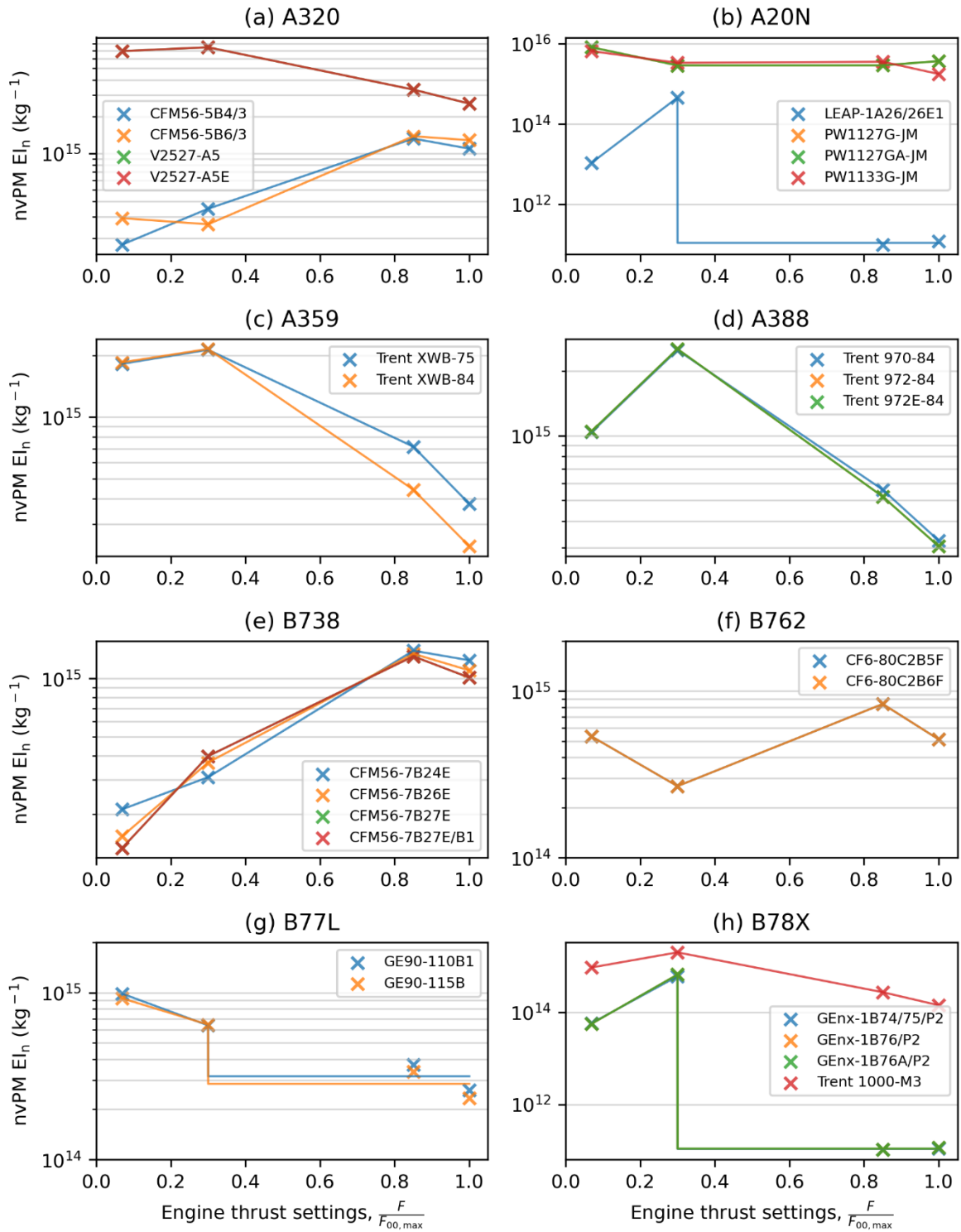


533

534

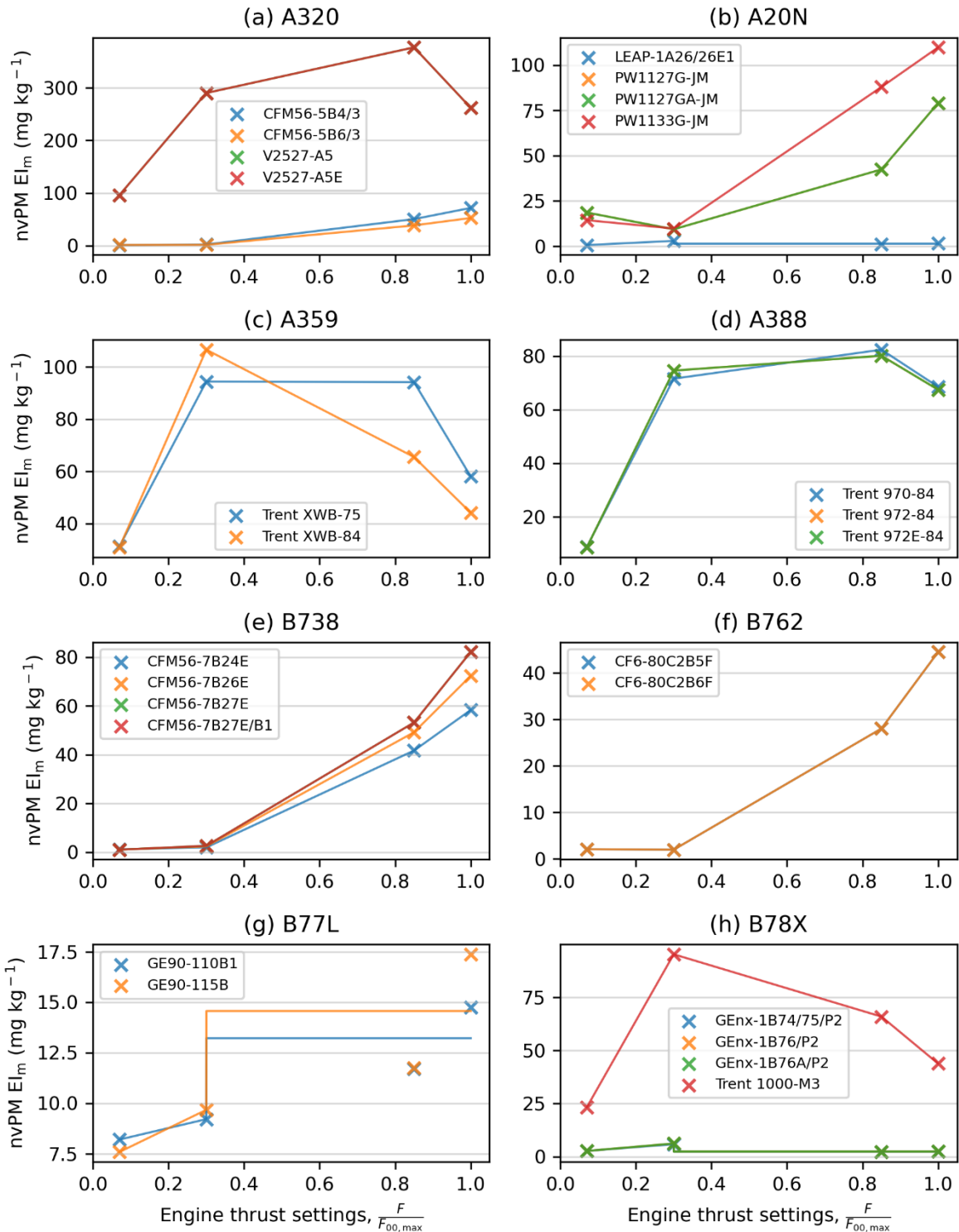
535

Figure S19: ICAO EDB measurements of the HC EI at the four certification test points (7%, 30%, 85% and 100% engine thrust settings) for selected aircraft-engine pairs.



536
537
538
539
540

Figure S20: ICAO EDB measurements of the nvPM EI_n that is corrected for particle losses at the four certification test points (7%, 30%, 85% and 100% engine thrust settings) for selected aircraft-engine pairs. The nvPM emissions profile for each engine (individual lines) is constructed using the methodology outlined in the SI §S4, which accounts for the step change in nvPM emissions from staged combustors.



541

542 **Figure S21: ICAO EDB measurements of the nvPM EI_m that is corrected for particle losses at the four**
 543 **certification test points (7%, 30%, 85% and 100% engine thrust settings) for selected aircraft-engine pairs.**
 544 **The nvPM emissions profile for each engine (individual lines) is constructed using the methodology outlined**
 545 **in the SI §S4, which accounts for the step change in nvPM emissions from staged combustors.**

546

547 **References**

- 548 Abrahamson, J. P., Zelina, J., Andac, M. G., and Vander Wal, R. L.: Predictive Model Development
549 for Aviation Black Carbon Mass Emissions from Alternative and Conventional Fuels at Ground and
550 Cruise, *Environ. Sci. Technol.*, 50, 12048–12055, <https://doi.org/10.1021/acs.est.6b03749>, 2016.
- 551 Airlines for America: World Airlines Traffic and Capacity: [https://www.airlines.org/dataset/world-](https://www.airlines.org/dataset/world-airlines-traffic-and-capacity/)
552 [airlines-traffic-and-capacity/](https://www.airlines.org/dataset/world-airlines-traffic-and-capacity/), 2022. Last access: 12 August 2022.
- 553 Boies, A. M., Stettler, M. E. J., Swanson, J. J., Johnson, T. J., Olfert, J. S., Johnson, M., Eggersdorfer,
554 M. L., Rindlisbacher, T., Wang, J., and Thomson, K.: Particle emission characteristics of a gas turbine
555 with a double annular combustor, *Aerosol Sci. Technol.*, 49, 842–855,
556 <https://doi.org/10.1080/02786826.2015.1078452>, 2015.
- 557 Bräuer, T., Voigt, C., Sauer, D., Kaufmann, S., Hahn, V., Scheibe, M., Schlager, H., Diskin, G. S.,
558 Nowak, J. B., DiGangi, J. P., Huber, F., Moore, R. H., and Anderson, B. E.: Airborne Measurements
559 of Contrail Ice Properties—Dependence on Temperature and Humidity, *Geophys. Res. Lett.*, 48,
560 e2020GL092166, <https://doi.org/10.1029/2020GL092166>, 2021.
- 561 Changi Airport Group: Changi Airport handled 68.3 million passengers in 2019:
562 [https://www.changiairport.com/corporate/media-centre/newsroom.html#/pressreleases/changi-airport-](https://www.changiairport.com/corporate/media-centre/newsroom.html#/pressreleases/changi-airport-handled-68-dot-3-million-passengers-in-2019-2966486)
563 [handled-68-dot-3-million-passengers-in-2019-2966486](https://www.changiairport.com/corporate/media-centre/newsroom.html#/pressreleases/changi-airport-handled-68-dot-3-million-passengers-in-2019-2966486), 2020. Last access: 16 August 2022.
- 564 Changi Airport Group: Traffic Statistics: [https://www.changiairport.com/corporate/our-expertise/air-](https://www.changiairport.com/corporate/our-expertise/air-hub/traffic-statistics.html)
565 [hub/traffic-statistics.html](https://www.changiairport.com/corporate/our-expertise/air-hub/traffic-statistics.html), 2022a. Last access: 16 August 2022a.
- 566 Changi Airport Group: Statistics for Singapore Airport: <https://singaporeairport.net/statistics/>, 2022b.
567 Last access: 16 August 2022.
- 568 Cirium: Aircraft fleets and values: the world’s largest independent aircraft database, 2022.
- 569 Cumpsty, N. A. and Heyes, A.: Jet propulsion: A simple guide to the aerodynamics and
570 thermodynamic design and performance of jet engines, Third Edition., Cambridge University Press,
571 2015.

572 Dalmau, R. and Prats, X.: Assessing the impact of relaxing cruise operations with a reduction of the
573 minimum rate of climb and/or step climb heights, *Aerosp. Sci. Technol.*, 70, 461–470,
574 <https://doi.org/10.1016/J.AST.2017.08.032>, 2017.

575 Dastanpour, R. and Rogak, S. N.: Observations of a correlation between primary particle and
576 aggregate size for soot particles, *Aerosol Sci. Technol.*, 48, 1043–1049,
577 <https://doi.org/10.1080/02786826.2014.955565>, 2014.

578 Döpelheuer, A. and Lecht, M.: Influence of engine performance on emission characteristics, in:
579 Symposium of the applied vehicle Technology Pane-Gas Turbine Engine Combustion, Emissions and
580 alternative fuels, Lisbon, Portugal, 1998.

581 DuBois, D. and Paynter, G.: Fuel Flow Method2" for Estimating Aircraft Emissions, *J. Aerosp.*, 115,
582 1–14, <https://doi.org/https://doi.org/10.4271/2006-01-1987>, 2006.

583 EASA: ICAO Aircraft Engine Emissions Databank (07/2021), 2021.

584 EUROCONTROL: User Manual for the Base of Aircraft Data (BADA) Family 4, 2016.

585 EUROCONTROL: User Manual for the Base of Aircraft Data (BADA) Revision 3.15,
586 EUROCONTROL Experimental Centre (EEC), 2019.

587 Heathrow Airport: Traffic Statistics: [https://www.heathrow.com/company/investor-](https://www.heathrow.com/company/investor-centre/reports/traffic-statistics)
588 [centre/reports/traffic-statistics](https://www.heathrow.com/company/investor-centre/reports/traffic-statistics), 2022. Last access: 16 August 2022b.

589 IATA: Industry Statistics: Fact Sheet (June 2022): [https://www.iata.org/en/iata-](https://www.iata.org/en/iata-repository/pressroom/fact-sheets/industry-statistics/)
590 [repository/pressroom/fact-sheets/industry-statistics/](https://www.iata.org/en/iata-repository/pressroom/fact-sheets/industry-statistics/), 2022. Last access: 15 August 2022.

591 IATA: Passenger Demand Recovery Continued in 2021 but Omicron Having Impact:
592 <https://www.iata.org/en/pressroom/2022-releases/2022-01-25-02/>, 2022. Last access: 17 August 2022.

593 ICAO: The World of Air Transport in 2019: [https://www.icao.int/annual-report-2019/Pages/the-](https://www.icao.int/annual-report-2019/Pages/the-world-of-air-transport-in-2019.aspx)
594 [world-of-air-transport-in-2019.aspx](https://www.icao.int/annual-report-2019/Pages/the-world-of-air-transport-in-2019.aspx), 2019. Last access: 15 August 2022.

595 ICAO: Overview of Automatic Dependent Surveillance-Broadcast (ADS-B) Out, 2021a.

596 ICAO: The World of Air Transport in 2020, 2021b.

597 ICAO: Air Transport Monitor: <https://www.icao.int/sustainability/pages/air-traffic-monitor.aspx>,
598 2022. Last access: 7 September 2022.

599 Park, K., Kittelson, D. B., Zachariah, M. R., and McMurry, P. H.: Measurement of inherent material
600 density of nanoparticle agglomerates, *J. Nanoparticle Res.*, 6, 267–272,
601 <https://doi.org/10.1023/B:NANO.0000034657.71309.e6>, 2004.

602 Peck, J., Oluwole, O. O., Wong, H.-W., and Miake-Lye, R. C.: An algorithm to estimate aircraft
603 cruise black carbon emissions for use in developing a cruise emissions inventory, *J. Air Waste*
604 *Manage. Assoc.*, 63, 367–375, <https://doi.org/10.1080/10962247.2012.751467>, 2013.

605 Port Authority of New York and New Jersey: Airport Traffic Statistics:
606 <https://www.panynj.gov/airports/en/statistics-general-info.html>, 2022. Last access: 16 August 2022.

607 Quadros, F. D. A., Snellen, M., Sun, J., and Dedoussi, I. C.: Global Civil Aviation Emissions
608 Estimates for 2017–2020 Using ADS-B Data, *J. Aircr.*, 1–11, <https://doi.org/10.2514/1.C036763>,
609 2022.

610 Schripp, T., Anderson, B. E., Bauder, U., Rauch, B., Corbin, J. C., Smallwood, G. J., Lobo, P.,
611 Crosbie, E. C., Shook, M. A., Miake-Lye, R. C., Yu, Z., Freedman, A., Whitefield, P. D., Robinson,
612 C. E., Achterberg, S. L., Köhler, M., Oßwald, P., Grein, T., Sauer, D., Voigt, C., Schlager, H., and
613 LeClercq, P.: Aircraft engine particulate matter emissions from sustainable aviation fuels: Results
614 from ground-based measurements during the NASA/DLR campaign ECLIF2/ND-MAX, 325, 124764,
615 <https://doi.org/10.1016/J.FUEL.2022.124764>, 2022.

616 Schumann, U., Penner, J. E., Chen, Y., Zhou, C., and Graf, K.: Dehydration effects from contrails in a
617 coupled contrail–climate model, *Atmos. Chem. Phys.*, 15, 11179–11199, [https://doi.org/10.5194/acp-](https://doi.org/10.5194/acp-15-11179-2015)
618 [15-11179-2015](https://doi.org/10.5194/acp-15-11179-2015), 2015.

619 Sobieralski, J. B. and Mumbower, S.: Jet-setting during COVID-19: Environmental implications of
620 the pandemic induced private aviation boom, *Transp. Res. Interdiscip. Perspect.*, 13, 100575,
621 <https://doi.org/10.1016/J.TRIP.2022.100575>, 2022.

622 Spire Aviation: Industry Leading ADS-B Data, n.d.

623 Stettler, M. E. J., Boies, A., Petzold, A., and Barrett, S. R. H.: Global civil aviation black carbon
624 emissions, *Environ. Sci. Technol.*, 47, 10397–10404, <https://doi.org/10.1021/es401356v>, 2013.

625 Stickles, R. and Barrett, J.: TAPS II Combustor Final Report. CLEEN Program, Washington, DC.,
626 2013.

627 Teoh, R., Stettler, M. E. J., Majumdar, A., Schumann, U., Graves, B., and Boies, A.: A methodology
628 to relate black carbon particle number and mass emissions, *J. Aerosol Sci.*, 132, 44–59,
629 <https://doi.org/10.1016/J.JAEROSCI.2019.03.006>, 2019.

630 Teoh, R., Schumann, U., Majumdar, A., and Stettler, M. E. J.: Mitigating the Climate Forcing of
631 Aircraft Contrails by Small-Scale Diversions and Technology Adoption, *Environ. Sci. Technol.*, 54,
632 2941–2950, <https://doi.org/10.1021/acs.est.9b05608>, 2020.

633 Teoh, R., Schumann, U., Gryspeerdt, E., Shapiro, M., Molloy, J., Koudis, G., Voigt, C., and Stettler,
634 M.: Aviation Contrail Climate Effects in the North Atlantic from 2016-2021.,
635 <https://doi.org/https://doi.org/10.5194/acp-2022-169>, 2022a.

636 Teoh, R., Schumann, U., Voigt, C., Schripp, T., Shapiro, M., Engberg, Z., Molloy, J., Koudis, G., and
637 Stettler, M. E. J.: Targeted Use of Sustainable Aviation Fuel to Maximise Climate Benefits, *Environ.*
638 *Sci. Technol.*, 56, 17246–17255, <https://doi.org/https://doi.org/10.1021/acs.est.2c05781>, 2022b.

639 Voigt, C., Kleine, J., Sauer, D., Moore, R. H., Bräuer, T., Le Clercq, P., Kaufmann, S., Scheibe, M.,
640 Jurkat-Witschas, T., Aigner, M., Bauder, U., Boose, Y., Borrmann, S., Crosbie, E., Diskin, G. S.,
641 DiGangi, J., Hahn, V., Heckl, C., Huber, F., Nowak, J. B., Rapp, M., Rauch, B., Robinson, C.,
642 Schripp, T., Shook, M., Winstead, E., Ziemba, L., Schlager, H., and Anderson, B. E.: Cleaner burning
643 aviation fuels can reduce contrail cloudiness, *Commun. Earth Environ.* 2021 21, 2, 1–10,
644 <https://doi.org/10.1038/s43247-021-00174-y>, 2021.

645 Wasiuk, D. K., Lowenberg, M. H., and Shallcross, D. E.: An aircraft performance model
646 implementation for the estimation of global and regional commercial aviation fuel burn and
647 emissions, *Transp. Res. Part D Transp. Environ.*, 35, 142–159,
648 <https://doi.org/10.1016/j.trd.2014.11.022>, 2015.

649 Wikipedia: ICAO airport code: https://en.wikipedia.org/wiki/ICAO_airport_code, last access: 7

650 September 2022.

651